2. Across-arc systematic geochemical zonation in trace elements and U/Th isotopes in Kamchatka and its probable causes

Churikova [1,2], T.; Dorendorf [1], F.; Woerner [1], G.; Eisenhauer [1], A.

[1)] Geochemisches Institut, Goldschmidtstr. 1, 37077 Göttingen, Germany
[2)] Institute of Volcanology and Geochemistry, Piip Avenue 9, Petropavlowsk, Kamchatka, Russia

Abstract

Major, trace and isotopic variations in mafic volcanics were studied in a 220 km wide transect across the Kamchatka arc from the Eastern Volcanic Front (EVF) over the Central Kamchatka (CKD) to the Sredinny ridge (SR). The dense sampling of 13 volcanoes and two cinder cone fields with varying positions from 110 to 400 km above the slab surface provides the opportunity to characterize the relative amount and composition of the slab fluid, introduced in the magma source.

High-K calcalkaline basalts and HFSE enriched within-plate basalts (WPB) occurring beside the typical low- to medium-K calc-alkaline arc rocks in the CKD and SR, respectively were separately studied.

Typical Kamchatka arc basalts, corrected for fractionation on MgO 8 %, display a strong increase in LILE (except Cs and Li), LREE and HFSE from the front to the back-arc. Ba/Zr- and Ce/Pb-ratios are nearly constant across the arc, which suggest a similar fluid input from the front to the back-arc. Similar melting degrees are probably from restricted $(CaO)_{8.0}$ – $(Na_2O)_{8.0}$ variations. Pb-isotopic ratios are MORB-like and do constantly decrease from the front to the back-arc. Sr is most radiogenic in the CKD, but almost similar in the EVF and the SR. A slight $^{238}U/^{230}Th$ disequilibrium > 1 could only be proved for the CKD, suggesting a recent (<300.000 a) U-enrichment by slab fluid in these rocks. This agrees with the highest U/Th ratios in CKD volcanics. In difference La/Yb and Nb/Zr constantly increase from the EVF above the CKD to the SR. This suggest, that the mantle source was inhomogeneously composed prior to fluid enrichment, reaching from depleted in the EVF and CKD to strongly

enriched in the SR. Modeling shows, that the enriched component is similar to an OIB source, which was overprinted by a similar fluid, like in the IAB.

Decreasing contents of Cs, Li and chalkophile elements suggest the depletion of the slab in these highly mobile elements in the early stages of dehydration.

The high-K calc-alkaline basalts occurring in the CKD were probably derived from a different source by lower melting degrees. The rocks from volcanoes of the Northern part of the CKD are significantly displaced from the trend and were obviously enriched by an adakitic component.

Introduction

New geochemical data provide evidence that the major source of arc magmatism is the mantle wedge above the subducted oceanic plate (e.g. Tatsumi and Eggins, 1995) and references therein). The melting of this source is triggered by interaction between the upper mantle rocks with slab-derived, hydrous fluids or/and melts (Davidson, 1996). Slab fluids are enriched in large ion lithophile elements (LILE, e.g. Cs, Rb, K, Ba, Pb) and LREE but depleted in high field strength elements (HFSE, e.g. Nb, Ta, Zr, Hf) and HREE. In rare cases, silica-rich melts are produced by partial melting of the subducted oceanic plate. Compared to fluids, such melts are enriched in all incompatible elements, i.e. also in the HFSE and strongly depleted in the HREE (Defant and Drummond, 1990).

Different attempts were made to constrain the slab fluid composition. The incompatible trace element pattern of primitive island arc volcanics was used by Pearce (1983) and McCulloch and Gamble (1991) to estimate the slab fluid contribution to the mantle source. However, a problem in these calculations is, that additional factors like differences in melting degree and contributions from subducted sediments, the subcontinental lithosphere or the crust may have a large influence on the trace element patterns. These factors may vary from arc to arc and are mainly related to crustal thickness, mantle fertility and the composition of the subducted plate (Pearce and Parkinson, 1993; Plank and Langmuir, 1988; Plank and Langmuir, 1993). The study of across-arc variations in major and trace elements and isotopes of primitive arc rocks has the advantage to control some of these variables. Such studies were performed successfully for Japan (Shibata and Nakamura, 1997) and the Kuriles (Avdeiko et al., 1991).

Previous studies of across-arc variations on Kamchatka (Hochstaedter et al., 1996; Kepezhinskas et al., 1997; Tatsumi et al., 1995; Volynets, 1994) gave rather ambiguous results, largely caused by the limited database. The Kamchatka Peninsula, forming the northern part of the Kurile-Kamchatka volcanic arc, is located in the northwest Pacific Ocean and represents one of the most volcanically active regions on the Earth. More than 200 Quaternary volcanoes, including 29 active ones, have been identified on Kamchatka. The worldwide interest for this area is caused by the fact, that in comparison with other volcanic arcs, recent and unaltered high-Mg rocks occur, which allows to study the processes of magma generation. Additionally it was shown previously (Kersting and Arculus, 1995; Tsvetkov et al., 1989; Turner et al., 1998), that the amount of the sedimentary component is very limited, offering the chance to investigate a relatively simple system.

In this study volcanic rocks from a densely sampled E-W transect have been analyzed for major and trace element compositions as well as isotopes of Sr, Nd, Pb, U and Th to assess the compositional changes across the arc and their possible reasons. The transect has the potential to test existing models of slab dehydration (Schmidt and Poli, 1998; Tatsumi and Eggins, 1995) and melt generation (Pearce and Parkinson, 1993; Plank and Langmuir, 1988).

Geological setting and sampling

The Kamchatka arc is located at the NE boundary between the Eurasian and Pacific plates, which are converging with ~9 cm/a. Active volcanism passes over continuously to the Kurile island arc in the south. The northern termination of volcanic activity at Shiveluch volcano is connected with the change of the plate geometry from a SW-NE convergent into a NW-SE transform plate boundary. The extinct 2-15 Ma old volcanism (Kepezhinskas et al., 1997), which occurred still further to the North was related to the short-lived spreading center in the Komandorsky basin (Baranov et al., 1991). Volcanic activity on Kamchatka is dated back to Cretaceous, however, the Recent plate-tectonic configuration was formed only in Late Miocene to Early Pliocene. Plateau basalts, partly with intra-plate characteristics, were formed from Pliocene to Lower Pleistocene. A remarkable intensification of volcanism is reported from Upper Pleistocene to Holocene (Erlikh et al., 1971).

Arc volcanism on Kamchatka (Fig. 2-1) comprises from E to W three zones parallel to the trench: (1) the Eastern Volcanic Front (EVF), (2) the Central Kamchatka zone and graben depression with the famous Kluchevskaya Group (CKD) and (3) the Western Volcanic Zone of the Sredinny ridge (SR). These zones correspond to the three chains investigated by Tatsumi et al. (1995). The SR represents the Miocene volcanic front, which switched in a back-arc position after the accretion of the Kronotzky terrane and the formation of the Recent active volcanic front. The present plate tectonic situation can be regarded as relatively stable at least since the Pliocene.

Deep seismic sounding investigations (Balesta, 1991) result in the following crustal and mantle profile. The crustal thickness of Kamchatka varies from 20 km to 40 km, increasing from the south to the north. Across the arc on the latitude of the Kluchevskaya Group of volcanoes the crust thickness varies from 30 km below Sredinny ridge to 40-42 km below Kluchevskoy volcano. The characteristic feature of the crustal section in the Kluchevskaya Group area is a thick (10-12 km) transitional zone from the crust to the mantle (Balesta, 1991). Evidence of the association of magma chambers with the crust-mantle transitional layer has been obtained by seismic studies of the lower crust and upper mantle below several Kamchatka volcanoes. Geophysical evidence suggests upper crustal magma chambers ranging in depth from 1.5-2.0 km below the Avachinsky and Tolbachinsky volcanoes to 10-20 km for Bezymianny volcano (Balesta, 1991). The depth of the seismic zone of the descending slab increases from 100-140 km below the Eastern Volcanic Front to 400 km below Ichinsky volcano (Fedotov and Masurenkov, 1991; Gorbatov, 1997). However, the dip angle of the slab flattens out in the north of the Kronotzky Peninsula at about 55°N, resulting in a shift of the volcanic front to the W. This change in the dip angle from 55° to 35° is connected with the subduction of the Meiji seamount chain, which forms the northern termination of the Hawaii-Emperor-ridge (Gorbatov, 1997). Geophysical results suggest, that the northern volcanoes of the CKD probably represent the northern continuation of the volcanic front. The Shiveluch volcano is located directly at the plate boundary of the pacific plate (Gorelchik et al., 1997).

We have sampled in detail a 220 km traverse of ten Upper Pleistocene and Holocene stratovolcanoes as well as several monogenetic cones in the north of Kamchatka peninsula from the frontal zone (Komarov, Gamchen, Shmidt, Kizimen, Tamara cone) through the Kluchevskaya Group (Kluchevskoy, Tolbachik, Ploskie Sopky, Kamen, Shiveluch, Kharchinsky, Zarechny, Nikolka) into the back arc with monogenetic volcanic centers at Achtang and Esso and the isolated Ichinsky stratovolcano. The distance from the volcanic front to the back-arc is a maximum worldwide. The rocks studied are mostly Upper Pleistocene to Holocene in age. Rare exceptions belong to the Pliocene to Lower Pleistocene plateau basalts and Middle Pleistocene shield volcanoes, which were sampled for comparison with the younger rocks. A description of the single areas, petrology and assumed rock ages is given in the appendix 1. The depth of the seismofocal zone is shown in Fig. 2-1.

Analytical techniques

Major elements and some trace elements were determined with the standard XRF analysis on glass disks, prepared with a sodium tetraborate flux. Fe_2O_3 was determined titrimetrically with $KMnO_5$ and the loss on ignition (LOI) by heating to 1100°C. Analytical errors for major elements are around 1 % (except for Fe, Na: 2 % and LOI: ~10%) and for trace elements around 5 %.

Additional trace elements were obtained by ICP-MS. About 100 mg whole rock powders were dissolved in teflon beakers with a mixture of HF and $HClO_4$ under pressure and after evaporation redissolved in HNO_3 for the measurement. The international standards JB3 and JA2 were analyzed continuously together with samples to check the external reproducibility. From this we estimate the error for Nb and Ta to about 15-20 %, for all other trace elements the error is lower than 10 %.

Isotope ratios of Sr and Nd were measured with a Finnigan MAT 262 RPQ II+ in Göttingen. The Sr- and Nd-isotope ratios were corrected for mass fractionation to $^{87}Sr/^{88}Sr$=0.1194 and $^{143}Nd/^{144}Nd$=0.7219 and referenced to NBS987 (0.710245) and LaJolla (0.511847). Measured values of these standards over the period of the study were 0.710262±24 and 0.511847±20. Lead isotopes were corrected to NBS981 (Todt et al., 1984). 13 measurements of this standard gave an average of $^{206}Pb/^{204}Pb$=16.90±0.01, $^{207}Pb/^{204}Pb$ =15.44±0.02 and $^{208}Pb/^{204}Pb$ =37.53±0.05. Blanks for Sr, Nd and Pb are <1ng, <0.03ng and <0.5ng, respectively, and have no influence on the results. From continuous measurement of standards and repeated measurements of samples, total errors (2σ) less than 0.004 % for Sr and Nd, and less than 0.1 % for Pb isotopes were determined.

For the study of the U-Th-disequilibrium only Holocene, mostly historic samples have been selected. Powdered samples of about 100 mg were spiked with ^{233}U, ^{236}U and ^{229}Th and dissolved similarly like for ICP-MS. Both U and Th fractions, obtained on anion resin columns with HCl and HBr acids were loaded on the same Rhenium double filament. Isotope measurements were performed on a Finnigan MAT 262 mass spectrometer equipped with an

RPQ-II filter. U-isotopes were measured in dynamic mode with the RPQ II. Th-isotopes were measured in static mode with ion counting of ^{229}Th, ^{230}Th and Faraday collection of ^{232}Th. Blanks, analyzed during the course of this study were normally < 0.5 ppb U and < 0.3 ppb Th, which has no influence on the results. The measured U and Th isotope ratios were corrected for mass fractionation relative to analyses of the internal standards U-112 and Santa Cruz, respectively, which were analyzed under the same operation conditions and at the same time as the samples. The basanite E-41 from Rothenberg volcano (Bourdon et al., 1994) was analyzed to check the external reproducibility. From these measurements, from the internal standards and double determinations of samples an external error of around 5 % in the U and Th activity ratios must be assumed. Some of the studied samples were previously analyzed by Chabaux and Allegre (1994) and Turner et al. (1998). Although their analyses where performed not from the same rock powder, they gave comparable results within error.

Results and discussion

Major and trace elements

Major and some trace elements have been analyzed by XRF for 178 samples and for additional trace elements by ICP-MS for 90 samples.

Rocks of the EVF, including Kizimen volcano are represented by low- to medium-K tholeiitic and calc-alkaline series (Fig. 2-2). Some rare low-K tholeiitic rocks exist at Gamchen and Shmidt volcanoes. The rocks of the back arc (SR) are medium to high-K calc-alkaline and correspond to calc-alkaline series in terms of SiO_2 - FeO*/MgO diagram (Fig. 2-3). At Ichinsky volcano HFSE enriched basalts with a within-plate characteristic (WPB) occur next to island arc basalts (IAB) (Volynets, 1994). In the basaltic rocks WPB are more abundant than the IAB rocks. From basalts with > 5 % MgO our collection only the samples 6250, ICH-19 and ICH-71 belong to the IAB series. The andesitic to rhyodacitic rocks of the stratovolcano are probably derived from IAB magmas. The highest variation in alkalis is observed for the CKD rocks. They are mostly medium-K calc-alkaline, but some samples of Ploskie Sopky and Nikolka volcanoes as well as some Al-basalts from Tolbachik, including these of the fissure eruption of 1976 are high-K calc-alkaline. They follow tholeiitic and calc-alkaline trends in the SiO_2 - FeO*/MgO diagram. At the northern volcanoes of the CKD, e.g.

the Shiveluch, Kharchinsky and Zarechny (named NCKD) high-Mg andesites occur, which were explained to contain a slab melt component (Kepezhinskas et al., 1997; Volynets et al., 1997a).

In difference to the Bakening area (Dorendorf et al., 2000a) no significant contrast exists in geochemistry between the Upper Pleistocene and Holocene rocks and the Lower Pleistocene plateau basalts.

The distribution of trace elements in the EVF, CKD and SR is shown in Fig. 2-4. For simplification we have only shown rocks with > 6 % MgO. The high-K calc-alkaline rocks, the rocks of the NCKD and the WPB are compared with the typical rocks of the corresponding regions. As we can see from NMORB-normalized spider diagrams (Sun and McDonough, 1989) the rocks have typical arc-signatures (except of several monogenetic cones around Ichinsky volcano, see below) with a strong and variable LILE and LREE enrichment but comparable low concentrations in the HFSE. The LILE and HFSE concentrations obviously increase to the back-arc. The HREE are much lower than in the NMORB and do not change significantly in the three groups. The rocks of the CKD and EVF are depleted in Nb and Ta compared to the NMORB. The high-K calc-alkaline rocks are enriched in all incompatible elements. The WPB at Ichinsky are more enriched in LILE and LREE than the IAB of the S and have especially higher HFSE concentrations. The Nb-Ta-depletion compared to the neighboring LILE is much smaller than in the IAB.

Fractionation correction

Mafic samples in the EVF, CKD and SR have MgO contents up to 8.5 %, 12.3 % and 9.2 %, respectively. Some samples of the CKD are close to a primary mantle-derived melt composition. However, all other rocks of the EVF and SR and most rocks of the CKD are obviously affected by some mineral fractionation and a direct comparison of absolute major and trace element concentrations is therefore impossible. In order to minimize the effects of fractional crystallization and possible crustal contamination on incompatible elements it is necessary to correct the raw data to a primitive magma composition.

For the data correction we choose the approach used by Plank and Langmuir (1988), with some substantial modifications described below. The data of each single volcano are plotted versus MgO and regression lines are drawn through the data. The intercept at 8 % MgO results in the fractionation corrected values for major and trace elements. This approach assumes a constant fractionation assemblage. Different ol/cpx ratios will cause some scatter, because olivine is more Mg-rich than clinopyroxene and the melt gets faster MgO depleted than for cpx-dominated fractionation. These differences result in different degrees of fractionation and consequently a variable absolute enrichment of incompatible trace elements. Incompatible trace element ratios are not changed. Plagioclase fractionation starts at about 5 % MgO as seen in distinct kinks in major element trends (Fig. 2-5). Magnetite fractionation starts at different MgO contents (Fig. 2-6) and is responsible for Ti-depletion in the higher evolved rocks. Only in mafic rocks a constant cpx/ol fractionation assemblage may be assumed. Therefore we have used only samples with > 5 % MgO to calculate the regression lines and we prefer to normalize on 8 % MgO instead of 6 % as used by Plank and Langmuir (1988). The corrected data is marked by an 8.0 suffix.

The K_2O/Na_2O ratio should not change during the early ol-cpx-fractionation and the regression lines should give subhorizontal lines in plots of MgO versus K_2O/Na_2O. This is the case for most of our volcanoes. However, samples of two volcanoes of the CKD, from Tolbachik and Ploskie Sopky, show a second trend of increasing K_2O/Na_2O with fractionation. This trend is probably related to crustal processes and these samples are excluded from the discussion of across-arc source differences. Also the NCKD volcanoes and the WBP at Ichinsky volcano will be discussed separately.

For some volcanoes only a few samples with > 5 % MgO exist. For the Ploskie Sopky, Shiveluch, Zarechny and Kharchinsky volcanoes and the island arc series of Ichinsky volcano our data were therefore combined with the data base of O.Volynets, which includes literature data and his unpublished results (available on request). Insufficient data > 5 % MgO is available for Nikolka, Kamen, Gamchen and the monogenetic cones of Achtang and Shmidt. It is not meaningful to extrapolate from low MgO contents of Nikolka, Kamen and Gamchen to the MgO content of 8 %. These volcanoes were therefore not used in the discussion of absolute element variations. For the cones of the Achtang and Shmidt area at least one mafic sample close to 8 % MgO is available, which is included for comparison.

Incompatible trace elements are well correlated with MgO, the relative deviation from the regression line in the range >5 % MgO is normally about 10-20 %, similar to the error of the MgO corrected data.

Across-arc major and trace element variations

The MgO 8 % normalized concentrations were combined with subduction zone parameters such as crustal thickness, the distance to the trench, and the depth of the slab surface. Pearce and Parkinson (1993) and Plank and Langmuir (1988) have shown, that the extend of melting, which influences the absolute major and trace element contents depends from the crustal thickness. Geophysical data for the Kamchatka crust are limited (e.g. Balesta, 1991). The results suggest increasing crustal thickness from the EVF to the CKD and a decrease further to the SR. This is somewhat unexpected, because the CKD is considered to be a rift-like structure, which should be related to crustal thinning. In any case, the reported slight variations in the crustal thickness from 30 to 40 km are not sufficient to generate the observed large trace element variations.

Trench distance and depth of the slab surface are roughly related. The worldwide similar position of the frontal volcanic zone at about 110-130 km above the slab surface argues that melting is caused by slab fluids, which were liberated by pressure sensitive dehydration reactions (see Schmidt and Poli, 1998; Tatsumi and Eggins, 1995 and references therein). Therefore we prefer the depth of the slab surface below the volcano (after Gorbatov, 1997) as a reference for regional variations.

The data are shown for selected major and trace elements and element ratios versus depth of the slab surface in Figs. 2-7 to 2-10. The high-K calc-alkaline and within-plate rocks, as well as the NCKD group are marked in the diagrams and will be discussed separately. Most MgO-normalized incompatible trace elements, i.e. HFSE (Zr, Nb, Hf, Ta), LILE (Sr, Ba, Rb, Be, Pb, U, Th), LREE, some major elements (K, Na) and certain element ratios (K/Na, La/Yb, Sr/Y, Nb/Yb) of the "normal" primitive arc rocks are strongly positive correlated with the depth of the slab surface. A negative correlation exists for Cs, Li and the HREE. Especially well correlated are K_2O, Ba, Sr and Rb, which normalized concentrations increasing more than 2 times from the EVF to the SR. A slightly different behavior is found for Na_2O, the LREE and HFSE, which all strongly increase from the EVF to the CKD but show a much weaker increase further to the SR. Ti and P show a similar behavior and are even depleted in the SR compared to the CKD. However, the magnetite and possibly apatite fractionation limits the reliability of trends for these elements. No correlations at all exist for Y and the HREE, which lie in a narrow range. The rocks of the CKD show comparably large scatter in incompatible elements, even if the high-K calc-alkaline rocks and rocks of the NCKD are excluded.

Regional variations in some compatible major (Si, Fe, Ca) and trace elements (Ni, Co, V, Sc) are drastically decreased when the data are normalized to $MgO_{8.0}$ rather than $MgO_{6.0}$. In most cases, therefore, compatible element variations are susceptible to fractionation rather than document source variations. Our results of the across-arc trends in incompatible elements are comparable with other arcs such as the Kuriles (Avdeiko et al., 1991) and Japan (Shibata and Nakamura, 1997).

The high-K calc-alkaline rocks, rocks of the NCKD and the WPB of the SR deviate in distinct elements from the trend formed by the “normal” arc rocks. The high-K calc-alkali basalts of Tolbachik and Ploskie Sopky volcanoes are strongly enriched in K_2O, TiO_2, P_2O_5, Rb, Ba, Cs, Li, Be, HFSE (Zr, Nb, Ta, Hf), Y and the REE compared to the “normal” rocks of the CKD. The rocks of the NCKD are enriched in SiO_2, Na_2O, K_2O, Ba, Sr, Rb, Pb, Th, U, LREE and depleted in the HREE and Y compared to volcanic centers of the EVF with a similar level above the slab surface. But even compared to the CKD they are strongly enriched in most of these elements. They have the highest Sr/Y and La/Yb ratios of the CKD, which corresponds to the idea, that they contain a slab, melt component. The HFSE elements have similar concentrations like in the typical CKD rocks. The WPB at Ichinsky have high concentrations of Na_2O, TiO_2, P_2O_5, Sr, in all HFSE and REE and are depleted in SiO_2 and Rb compared to the Ichinsky IAB. The HFSE concentrations are extremely high compared to all other studied rocks. Consequently, they have high Ce/Pb, La/Yb and low U/Th and Ba/Nb ratios.

Sr-, Nd-, and Pb-isotopes

The isotope data for the transect are summarized in Tab. 2-1 and Fig. 2-11. The data plot close to the MORB field and variations in all isotope systems are small and inside the previously reported ranges for Kamchatka (Kepezhinskas et al., 1997; Kersting and Arculus, 1995; Tatsumi et al., 1995; Turner et al., 1998).

However, with more extensive and representative sampling, we can identify within this field different regions and in some cases even single volcanoes, which have distinct isotopic characteristics. There is a general increase in $^{87}Sr/^{86}Sr$ and $^{143}Nd/^{144}Nd$ from the EVF to the CKD and a decrease from the CKD to the SR (Fig. 2-12). The fields of the EVF and SR are nearly identically in Sr-Nd-isotope space, except for two samples from Komarov volcano, with slightly higher Sr-isotope ratios. A large range exists in Nd-isotopes for the EVF and SR compared to the relatively narrow range in Sr-isotopes. The highest radiogenic Sr enrichment in the CKD is found for the Kluchevskoy lavas with ratios up to 0.70366. The high-K calc-alkaline basalts and the high-Mg andesites of the NCKD are on average lower in Sr- and similar in Nd-isotopic ratios compared to the other CKD rocks. In Pb-isotopes we found a steady decrease from the EVF over the CKD to the SR. The high-K calc-alkaline basalts are significantly displaced to unradiogenic Pb-isotopic compositions. The Shiveluch sample from the NCKD has Pb-ratios comparable to the "normal" CKD rocks. Also, the WPB rocks are identical to the other rocks of the SR. The data for the Bakening volcano, studied by (Dorendorf et al., 2000a) is are for comparison in Fig. 2-12, which are even more unradiogenic in Sr at comparable Nd- and Pb-isotopic ratios. The field of xenolith data for Kamchatka (Koloskov et al., 2000) shows for Nd-isotopes a comparable and for Sr-isotopes an even larger range, than observed in the volcanic rocks.

U/Th systematic and U/Th disequilibrium

The fractionation of the U/Th ratio in the mantle results in the generation of a disequilibrium in the U-Th-Pb decay series, which can be used to detect fluid enrichment or melting processes (e.g. Hawkesworth et al., 1997). One assumption of this method is, that the time passed since this process is < 300.000 years. The U/Th ratios of all Kamchatka rocks are higher than in NMORB and range generally between 0.4 to 0.55, 0.55 to 0.7, 0.45 to 0.7 and 0.35 to 0.4 for the EVF, CKD, SR (IAB) and SR (WPB), respectively. One remarkable outlier in the CKD is sample 2310 from Kamen volcano with an U/Th ratio of 0.86, the highest ratio found in any primitive basalt of Kamchatka. This large ratio is coupled with extremely low U- and Th-concentrations.

The U-Th isotope data are presented in the diagram (^{230}Th/^{232}Th) versus (^{238}U/^{232}Th) (Fig. 2-13). The variation in (^{238}U/^{232}Th) is comparable with the discussed U/Th variation. The data scatter around the equiline and a maximum disequilibrium is at around ±10 %. This variation does not exceed much the proposed analytical error. However, the samples of the different regions show a consistent pattern from ^{238}U/^{230}Th < 1 to ^{238}U/^{230}Th > 1, clearly outside the analytical error. All samples from the EVF plot to the right of the equiline with a relative Th-enrichment of up to 9 %. CKD rocks are in difference enriched between 0 and 8 % in U over Th, except of the high-K calc-alkaline rocks, which show a relative Th enrichment of a similar degree. The sample from NCKD (Shiveluch) is also strongly U-enriched (9 %). All samples of the SR, except one sample have an excess of up to 10 % Th. The exception is sample ICH-64, which is relatively U-enriched. This sample is a highly evolved dacite of the Ichinsky stratovolcano with 67.4 % SiO_2 and therefore probably influenced by crustal processes. However, similar variations were also obtained from the Andes (Bourdon et al., 1999), where the rocks of the stratovolcano are U-enriched in difference to the adjacent monogenetic cones, which are Th-enriched. There exist no difference between the results for WPB and IAB of Ichinsky volcano.

U-enrichment over Th is generally attributed to a slab-derived fluid. A negative U-Th disequilibrium is widely attributed to partial melting in the presence of residual garnet in their mantle source (Hawkesworth et al., 1997).

Interpretation

Geochemical zonation across Kamchatka and possible causes

A strong geochemical zonation across the arc was shown for major and trace element from the EFV over the CKD to the SR (Figs. 2-7 to 2-10). The continuous trends across the arc can be only explained by a single subduction zone beneath Kamchatka volcanic arc, i.e. subduction of the Pacific oceanic plate below the Eurasian continental plate, which is confirmed by geophysical data (Fedotov and Masurenkov, 1991).

The normalization procedure ensures that the trends are representative of the primary magmas leaving mixing of depleted/enriched mantle sources with slab-derived hydrous fluids, water-rich melts or sediments from the slab as possible causes. Decreasing degrees of melting at increasing pressures further away from the volcanic front and the decreasing fluid flux from the slab due to “drying” of the subducted oceanic plate, will have an opposite effect on the LILE in the magma. It is very important to clarify which of all these processes control the across-arc variations and which of them have a secondary influence.

Using Pb and Be isotopes data it was evidenced (Kersting and Arculus, 1995; Tsvetkov et al., 1989), that subducted sediments play a minor role in magma generation in Kamchatka volcanic rocks. Additionally it was shown by the variation in Sr and O isotope data that the fluid is largely derived from the altered oceanic crust of the slab (Dorendorf et al., 2000b).

The further discussion of element variations is only restricted to MgO-normalized absolute element concentrations and incompatible element ratios of basaltic rocks (> 6 % MgO).

Isotope data comprise also a few higher evolved rocks, which are however, in general similar to the mafic rocks of the same suite.

Melting process

The melting degree has a large influence on absolute element concentrations. Decreasing melting degrees of a mantle consisting of olivine, orthopyroxene and clinopyroxene, result in enriched but subparallel patterns of incompatible elements in the melt. Only for very low melting degrees (< 5 %), which is not appropriate for most island arc lavas (Plank and Langmuir, 1993) the very high incompatible elements may be fractionated from each other. Residual garnet in the mantle can also strongly influence HREE and Y, because it buffers these elements in the melt on a comparable low level until it is completely consumed. The relatively low and uniform HREE and Y contents in our rocks (Fig. 2-4) can be an indication, that garnet was present at least at the beginning of melting.

Plank and Langmuir (1988) have argued that the thickness of the mantle wedge (distance between the crust and the slab surface) below the active volcanic front in arcs world-wide is directly linked with the melting degree, which is expressed in a negative correlation between $Ca_{6.0}$ and $Na_{6.0}$. The reason for such a trend is, that Ca is retained by clinopyroxene in the mantle residue and Na not. In our study we should see a clear variation because the mantle wedge thickness increases strongly from the EVF to the SR. A general correlation is detected in fact for the whole Kamchatka data (Fig. 2-14). Data corrected for 6 % MgO (Plank and Langmuir, 1988) give values, which are much more scattered than for the MgO 8 % (Fig. 2-14). The MgO 6 % corrected data overlap the field of Plank and Langmuir (1988) and extend it slightly to higher Na-concentrations. The higher $Na_{6.0}$ values are caused by the WPB and the rocks from the NCK. This would argue for comparably lower melting degrees in these rocks. For the other “normal” arc rocks and high-K calcalkaline basalts, the spread is very limited and not related to the depth of the slab surface (Fig. 2-14). A slight decrease of melting can be assumed from the EFV to the CKD and a constant melting degree from the CKD to the SR. Such almost similar melting degrees can be explained if the melting process is separated in two single stages (Pearce and Parkinson, 1993). First melting stage results from the fluid influx into the mantle. A second stage of melting results from decompression at shallower depth and will proceed as far as the MOHO. For the almost uniform crustal thickness across Kamchatka this second stage should be similar. The extend of the first stage depends from the amount of water in the source (Stolper and Newman, 1994) and can be estimated by the relative enrichment of incompatible elements in the source. This and other factors beside the melting degree, which can also cause the Ca-Na-variations, like a different fertility of the mantle or the mixing with slab melts (probably the case for the NCKD) will be discussed in the next chapters.

Variations in the amount and composition of the slab-derived hydrous fluid

The recent experimental data (Tatsumi et al., 1986) provide evidence that the melting of the primary mantle source is triggered by interactions between the upper mantle and hydrous fluids derived by dehydration of the subducted oceanic crust. According to mineral-melt partition coefficient data (Ayers, 1998; Brenan et al., 1995) such fluids should be rich in LILE (K, Cs, Rb, K, Ba, Pb), less enriched in LREE and relatively depleted in HFSE (Nb, Ta, Zr, Hf), Th and HREE. This is compatible with the pattern in arc volcanics and across-arc trends (e.g. Gill, 1981; Tatsumi and Eggins, 1995 and references therein).
Incompatible trace element ratios are an appropriate tool to study such enrichment processes, because they largely avoid the influence of different degrees of melting and fractional crystallization. Certain ratios between fluid mobile and immobile trace elements are shown in Fig. 2-10 in relation to the depth of the slab surface. The Ce/Pb ratio was shown to reflect the degree of fluid enrichment, because Pb is highly mobile in slab fluids (Miller et al., 1994). There is no systematic change in that ratio in relation to the depth of the slab surface. In all three regions Ce/Pb is about 5.0. The Kizimen volcano of the EVF and the WPB of the SR deviates to higher Ce/Pb ratios, suggesting a relatively lower fluid input. However, considering the La variations (Fig. 2-9 C), it is obvious, that this deviation is rather caused by the higher LREE contents.
Also the Ba/Zr (Fig. 2-10 D) and Ba/La (not shown) ratios indicate that the degree of fluid enrichment does not significantly change from the frontal zone to the back-arc. However, we must keep in mind, that the LREE and HFSE concentrations are also influenced by source depletion/enrichment (we will further discuss this in the chapter about source differences). This problem can be partly avoided, when we consider radiogenic isotope variations. If the slab fluid differs in Sr- and Pb-isotopic ratios from the mantle (which can be at least assumed for Sr in the altered oceanic crust), high proposed concentrations of these elements in the fluids will strongly influence the ratios in the metasomatized mantle. There exists a constant

decrease in Pb ratios from the frontal zone to the back arc (Fig. 2-8 D), which would suggest a decreasing influx of fluid across the arc. However, also limited amounts (< 1 %) of sediment in the source of the frontal lavas, which cannot be entirely excluded, can cause this trend. Sr- and Nd-isotopic ratios are not so sensitive because of relatively higher amounts of these elements in the mantle. This can explain, that Sr behaves differently, because in average the isotopic ratios increase from the EVF to the CKD and then decrease strongly to the SR. This suggests the highest amount of the slab-derived component in the CKD. The U/Th ratios (Fig. 2-10 E) and results of the U-Th disequilibrium study (Fig. 2-13) confirm this interpretation. Samples of the CKD have highest U/Th ratios and a disequilibrium, which is attributed to a recent (< 300.000 years) U-enrichment by a fluid.

The study of across-arc variations in the fluid influx is complicated by the fact, that the slab fluid composition will change depending from the extend of dehydration and residual minerals in the slab residue. Bebout (1995 and Noll et al. (1996) have shown, that certain chalkophile elements (As, Sb), B and Cs are highly enriched in the fore-arc and get depleted to the back-arc, caused by their extremely high mobility in fluids. Our results confirm this finding. Cs is highly concentrated in the EVF and decreases to the CKD and SR. Less pronounced but comparable is the behavior of Li, which decreases from 8-10 ppm to ~6 ppm, which is still enriched compared to MORB (Sun and McDonough, 1989). Also the chalkophile elements As and Sb have high enriched concentrations in the EVF and CKD and MORB-like concentrations in the SR (Heuser et al., 2000).

Different models exist about the mineral composition and dehydration of the subducting slab (Schmidt and Poli, 1998; Tatsumi and Eggins, 1995). With our data we can test, whether the pressure dependent dehydration of certain phases like amphibole, phengite or lawsonite are reflected in a changing fluid composition. The high concentrations of Rb, K, Ba and Sr in arc magmas can be an indication, that amphibole has retained these elements from early dehydration and provides them to the mantle, when it dehydrates at 60-70 km depth.

The dehydration of phengite should be reflected by a strong flux of Rb into the mantle, which should be easily detectable by a decreasing K/Rb ratio. This ratio is variable in mafic rocks of the EVF (300-600) and CKD (400-600) but relatively constant in the IAB of the SR (460-520). The high-K calc-alkaline rocks have slightly lower (320-340) and the WPB (~600) slightly higher ratios than comparable rocks in these regions. Phengite cannot be proved by our data in difference to Tatsumi et al. (1995) but corresponding with the data of other arcs (Gill, 1981).

Lawsonite strongly concentrates the REE (Tribuzio et al., 1996). The strong increase in the LREE can be the result of the dehydration of lawsonite, which was shown to be stable up to 10 GPa (Schmidt and Poli, 1998). The LREE/HREE enrichment is then caused by the slab fluid, which preferentially transports the LREE to the source. However, an increase in La and the La/Yb ratio can be also be explained by other processes like decreasing melting degrees with garnet in the residue or by an enriched mantle source.

Slab melts and source of the NCKD volcanoes

The samples of the NCKD (Shiveluch, Zarechny, Kharchinsky) were included in our transect, because evidence exists for a slab melt component in their source (Kepezhinskas et al., 1997; Volynets et al., 1997a). This is proved by their high Ba, Sr and La concentrations and high ratios of $(Sr/Y)_{8.0}$ of ~ 30 and $(La/Yb)_{8.0}$ of ~5 (Fig. 2-10 A), which exceed by far the compositions expected from the across-arc trends. Such a pattern is typical for adakites, for which is assumed that they were derived from slab melting (Defant and Drummond, 1990). The unusually high values of $(SiO_2)_{8.0}$, $(K_2O)_{8.0}$ and $(Na_2O)_{8.0}$ are also arguments that alkali-rich adakitic melts are a component in the NCKD source. Comparable HFSE contents in the NCKD and the “normal” CKD rocks indicate, that the HFSE were not enriched in the slab melt. This implies, that sphene or another phase with high $D_{mineral/melt}$ for the HFSE, retained these elements in the slab. The genesis of these adakites was discussed to be related to the special plate configuration below the NCKD volcanoes (Volynets et al., 1997a), where the edge of the Pacific plate melts by hot mantle material superimposed to it at the tear of the slab. However, for all other localities we can certainly exclude slab melting from thermal arguments. The fast subducting Pacific plate is considerable old (~100 Ma), which makes it impossible to melt at normal geothermal conditions in the mantle (Peacock, 1993).

It could be argued, that slab melting could be possible at least in the back-arc. Our trends prove however, that the SR rocks (except WPB) are not adakitic in character. The WPB are relatively enriched in Sr, Na, La, the HFSE, Ce/Pb and La/Yb. They do not show higher Sr/Y and Ba/Zr ratios, compared to the other SR rocks. The strongest argument is, that they are depleted in $(SiO_2)_{8.0}$ which excludes that the discussed enrichments are related to an adakitic melt.

Mantle source variations prior to fluid addition

The fertility of the mantle source is expressed in the slope of the trace element pattern in spidergrams, which depends on the relative incompatibility decreasing from the left to the right. This pattern is not much changed by moderate degrees of melting, which makes it possible to infer source composition from the melt (compare e.g. OIB in Fig. 2-4 E). However, most elements were additionally influenced by the fluid addition. Only for HFSE and HREE is assumed that they have low concentrations in the fluid (Ayers et al., 1997; Brenan et al., 1995; Stalder et al., 1998). These elements were used by Pearce and Parkinson (1993) to estimate the degree of depletion or enrichment of the source prior to fluid addition. For our samples there exists a steady increase in HFSE from the volcanic front to the back-arc suggesting source enrichment in this direction (or alternatively a source depletion in direction to the frontal arc). This pattern can be alternatively explained with decreasing melting degrees in the back-arc, which would fit to the proposed limited fluid-influx for the SR. Therefore ratios of very high and less incompatible HFSE or REE are more appropriate to study the fertility of the source, because they are almost not influenced by melting but strongly by depletion or enrichment events. The Nb/Yb ratios (Fig. 2-10 E) show that the sources of the EVF and CKD magmas are nearly identical and similar to a MORB source. By contrast the SR magmas have slightly higher ratios, especially for the WPB of Ichinsky. This cannot be the effect of garnet (which depletes Yb compared to Nb) because a similar behavior is found for the Nb/Zr ratios. That means, that an enriched mantle component exists below the SR.

The diagram of Th/Yb versus Ta/Yb was used by Pearce (1983) to distinguish between primitive island arc rocks from depleted sources and rocks from continental arcs from enriched sources (Fig. 2-15). The displacement from the mantle field to higher Th/Yb ratios is caused by fluid enrichment in Th, whereas the fertility of the source is shown by a similar enrichment in both ratios. All samples from the EVF and the CKD fall into the field of oceanic arc rocks close to the boundary between the tholeiitic and calc-alkaline field. However, the SR rocks form an array reaching from the oceanic arc into the continental arc field, which expresses obviously a mixing array between the depleted EVF and CKD field and an enriched mantle component. The WPB of the SR plot more closely to the mantle field, suggesting a lower proportion of the fluid component.

Before we discuss the reasons for this enrichment, we need to consider an alternative explanation for the observed HFSE enrichment in the back-arc. Below the SR fluids are liberated at higher temperatures and pressures from the slab, i.e. conditions, where probably

HFSE-retaining phases are not longer stable in the slab. Additionally high-P-T fluids have larger solute contents, which enhance their capability to transport HFSE (Brenan et al., 1995). The fluid calculated by Stolper and Newman (1994) for the enrichment in back-arc basalts probably is also highly enriched in Y and has a Ta/Y ratio twice than in the NMORB source. We can predict this also for the Nb/Yb ratio because Nb and Yb behave similarly to Ta and Y in the mantle. It is not possible to explain the compared to NMORB about 10 times enriched Nb/Yb ratios in the WPB of Ichinsky by such fluids.

The enriched component – OIB-source or lithospheric mantle?

From Th/Yb versus Ta/Yb we can assume, that despite our so-called WPB are unusually for the Kamchatka environment, the pattern is not unusually for continental arcs. Kamchatka represents an active continental arc with a relatively thin continental crust. The present subduction zone formed in the Late Miocene and it is likely, that the lithosphere below the SR, which was already influenced by an older subduction system, is more enriched. (Pearce, 1983) explains the within-plate signature in continental arc basalts by a significant contribution from such trace element enriched metasomatized subcontinental lithosphere. This seems plausible, because island arc volcanics do not show such enriched patterns (Fig. 2-15). However, also rare alkalic oceanic arcs exist, which are alternatively explained by an OIB-type source composition. Volynets et al. (1997b) could prove for Miocene WPB of East Kamchatka by Sr- and Nd-isotopes, that they contain a significant EM1 component. The Zr/Y ratio plotted versus Zr (not shown) is proposed by Pearce (1983) to distinguish between within-plate and alkali enrichment. Our rocks of the SR plot outside the proposed fields but are close to oceanic island basalts. The Nb/La versus Zr/Ba ratio was used by Molzahn et al. (1996) to differentiate between the lithospheric (high Nb/La) and the asthenospheric (low Nb/La) component. The regions of our transect form distinct groups with increasing Nb/La ratios in the CKD and high ratios in the SR (Fig. 2-16). The EVF is situated between these two fields. Additionally shown are OIB and MORB composition (Sun and McDonough, 1989) and the probable fluid composition. The ratios in the slab fluid can be roughly estimated from experimental data of Brenan et al. (1995; Stalder et al. (1998) to have relatively low Nb/La and Zr/Ba ratios. From models of fluid percolation (Hawkesworth et al., 1993; Navon and Stolper, 1987) we assume, that the composition of this fluid is changed by interaction with the mantle towards higher Zr/Ba ratios. The trend in the data reflects mixing between the slab fluid, a NMORB source and an OIB source. The SR rocks lie on a well-defined curve, between the fluid and the OIB source. The CKD rocks are more likely derived from a fluid enriched MORB source. The EVF is then a mixture between MORB and OIB sources. However, given a lower Zr/Ba ratio and higher Ba concentration in the EVF fluid close to the trench a mixture between the fluid and the MORB is also possible.

Different source should also be detectable in isotopes. Fig. 2-12 shows an isotope compositional field where the data is distributed in 3 directions. The component low in $^{87}Sr/^{86}Sr$ (<0.7031) and high in $^{143}Nd/^{144}Nd$ (~0.5131) is the MORB source. From the MORB field one array tends to higher Sr-ratios with unchanged Nd-ratios. This component is radiogenic in Sr- and an Nd-isotopic composition similarly to MORB (or alternatively with relatively low Nd-concentrations. Slab fluids have such expected composition. The second array begins from a point on the first trend (i.e. an fluid enriched MORB composition) and tends to low Nd-isotope ratios with only slight increase in Sr-isotopic composition. Such a trend probably results from mixing with the OIB component. This trend is formed by the SR and some EVF rocks, which support this interpretation that some enriched component exists in both sources.

High-K calc-alkaline basalts of the CKD

High-K calc-alkaline basalts occur at Tolbachik and Ploskie Sopky volcanoes in the Kluchevskaya Group beside the “normal” volcanics. They are enriched in all incompatible elements, except Sr relative to the “normal” CKD rocks (Fig. 2-4) and therefore fall off the across-arc trend in most geochemical parameters. The trace element patterns of the high-K calc-alkaline rocks are parallel to the other CKD rocks, which suggests, that they were produced by fractional crystallization from the same primitive magma. The Rb/Sr and K_2O/Na_2O ratios increase steadily with fractionation between 9 to 6 % MgO. Therefore the trace element enrichment seems to be connected with crustal contamination.

However, there are reasons to believe in a different source composition. In Fig. 2-15 the high-K calc-alkaline rocks are displaced from the CKD rocks to an enriched composition with higher Ta/Yb and Th/Yb ratios. Also the K/Rb ratios are significantly lower in the high-K calc-alkaline rocks. The lower Sr- and Pb-isotopic ratios in the high-K calc-alkaline basalts compared to the other CKD rocks are a strong argument for a different source composition. From low $(Sr/Y)_{8.0}$ and $(La/Yb)_{8.0}$ we can exclude an adakitic component in the source. An

OIB component in the source like that in the source of the SR rocks is not likely from Zr/Ba versus Na/Ba and the relatively low HFSE contents.

Our data provide the evidences that prior to the subduction slab fluid enrichment the high-K calc-alkaline rocks of the CKD had a less depleted mantle source compared to other rocks of the Kluchevskaya Group.

Model for magma generation across the Kamchatka arc

We have shown, that different processes played a role in the incompatible trace element enrichment across the arc. We want now combine the results in a model of magma generation in the Kamchatka arc.

It was shown, that subarc mantle is depleted similar like the MORB source with exception of the SR, whose source is reenriched to different extends with an OIB component.

The fluid enrichment from the slab can be calculated for the SR magmas, if the within-plate pattern is subtracted from the trace element pattern (Pearce, 1983), which is shown in Fig. 2-17. Our WBP was calculated as a mixture between 25 % OIB and 75 % MORB of Sun and McDonough (1989). The mixing ratio is fitted by the HFSE concentrations, assuming that the fluid did not carry any significant amount of these elements. It was not possible to fit the low HREE by this procedure. Such pattern is not only restricted to the WPB but to all other studied samples from Kamchatka as well. It is out the scope of this paper to discuss the reasons for this depletion, however, because the HREE are not fluid-mobile, we can neglect them in this context. The peaks above the within-plate baseline are caused by the fluid. Adding this fluid component to the MORB composition, we can compare it with rocks derived from fluid enriched MORB. The pattern is surprisingly similar shown in Fig. 2-17 B. Of cause there are additional factors like differences in melting degree or mantle mineralogy, which can influence the results. The good agreement suggests, that these factors are of minor importance. The other localities contain as maximum around 5 % OIB-component in their source, which has influenced the HFSE and the LREE but certainly not on the LILE, carried by the fluid. Therefore we assume that the across-arc variations in the LILE are not caused by source differences prior the fluid enrichment.

If we extrapolate WPB and IAB of Ichinsky, we can estimate the composition of the unenriched mantle source prior to fluid infiltration. This leads to a decrease in the concentrations of Sr, Be, Zr, Nb, La, Yb, Ti, Na and in the Ce/Pb, La/Yb, Nb/Yb ratios of the

IAB in the SR. However, regarding the 5 % OIB component in the IAB of SR in comparison with the 25 % OIB component in the WPB it is obvious that there is no substantial change in the pattern of the IAB

The U/Th and Ba/Zr ratios and the Sr-isotopic ratios have maximum values in the CKD. The EVF and SR rocks have comparable lower Ba/Zr, U/Th, Ce/Pb and Sr-isotope ratios and similar ratios. This indicates that the fluid input increase from the EVF to the CKD and than decrease further to the SR.

Conclusions

1. Major and trace elements in all studied samples except several within-plate like monogenetic cones in the back arc are typical for arc rocks. The systematic variations from the volcanic arc front at Komarov volcano to the back-arc at Ichinsky volcano clearly argue for a single subduction zone, contradicting earlier models.

2. Three parameters have mainly affected the observed geochemical zonation across the arc: (1) variable depleted primary mantle sources; (2) the fluid flux from the slab to the mantle source; (3) variable degrees of melting.

3. Variable depleted mantle sources exist below Kamchatka, from slightly depleted (EVF, CKD) to significantly enriched (SR) compared to a NMORB source. The depletion is possibly related to earlier MORB- or intra-arc rifting and melting events, which produced, for example, extensive plateau basalts and andesites in the Lower Pleistocene.

4. The within-plate basalts in the SR contain a significant contribution of a strongly HFSE enriched OIB-component (~50 %) in their source. The other rocks of the SR also have up to 5 % of OIB component.

5. The contribution from the slab is nearly identical across the arc. An exception is the CKD with a higher proposed fluid flux (enriched Sr-isotopic composition, higher U/Th and Ba/Zr ratios). The U-series disequilibrium in rocks of the CKD is caused by a recent enrichment of U over Th related to a higher fluid flux. This is relates to the high magma production rate in the CKD. Highly fluid mobile elements (Cs, Li, As, Sb) show decreasing concentrations across the arc, which can be most easily explained by the depletion of the slab in the earliest stages of dehydration in these elements.

6. An influence from slab-derived melts is found for the NCKD volcanoes (Shiveluch, Kharchinsky and Zarechny), where it is caused by superimposing hot mantle wedge and subducted slab along the subducted transform fault.

Appendix

Regional geology and sample description

The good introduction in the geology and history of most of the studied volcanoes is given in Fedotov and Masurenkov (1991). The ages in the text are mainly based on this publication, our field observations and the Russian geological maps 1:200.000.

Eastern volcanic front (EVF)

The EVF forms a continuous band of more than 20 active and hundreds of extinct volcanoes parallel to the trench. We have sampled the Northern part in detail, i.e. the Upper Quaternary to Holocene stratovolcanoes Gamchen, Komarov and Kizimen as well as monogenetic cinder cones superimposed on the Shmidt volcano and the Tamara cinder cone.

Shmidt volcano (SHM)

The eroded Lower Pleistocene (Q_1) Shmidt volcano is one of the largest shield volcanoes on Kamchatka (Vazheyevskaya et al., 1990). Around 30 Holocene monogenetic cinder cones are developed at its crest along NW-SE directed faults. Our samples are high-Mg ol-cpx-plag-phyric basalts and plag-phyric andesites from these Holocene cones.

Gamchen volcano (GAM)

The Late Pleistocene Gamchen volcano in the north of Shmidt volcano is a composite volcano consisting of the Northern Gamchen (2344 m), Southern Gamchen (2569 m) and volcanoes Molodoy and Barany. They are composed of relatively uniform andesite flows and tuffs with plag, cpx and rarely ol. Amph was found in the extrusion at the E-slope of Molodoy. The basement of Gamchen is formed by the Middle Pleistocene (Q_2) Menner shield volcano with a basaltic to andesitic composition. Up to some cm-large xenocrysts of ol and cpx occur sporadically in sample GAM-28. The Pliocene plateau basalts, occurring in the SW, look alike the younger rocks. Rocks of the plateau basalts and the Menner shield volcanoes were sampled for comparison with the stratovolcano.

Komarov volcano (KOM)

The Komarov volcano (2059 m) was formed in Upper Pleistocene to Holocene times. Ol-cpx-phyric basalts form the eroded caldera at the SE base of the stratovolcano. The stratovolcano is largely composed of up to 5 km long andesitic lava flows with abundant plag, cpx and occasionally ol.

Kizimen volcano (KOM) and Tamara cinder cone (TAM)

The Kizimen volcano (2376 m) is situated between the EVF and CKD, which are 30 km and 40 km away, respectively. The volcano consists of several extrusive domes and lava flows of different composition (plag, amph, occasionally ol, cpx and qz). Four main periods of volcanic activity are distinguished in the volcano history from 12.000 to 8400 a, 8400 to 6400 a, 6400 to 3000 a and 300 a to present time (Melekestsev et al., 1995). Each period started with strong explosive eruptions and finished with the forming of an extrusive dome and lava flows. The composition of the rocks is changed with time from dacite to basaltic. According to the previous study, a nonequilibrium mineral association (qz and Mg-ol phenocrysts in andesites and dacites) shows the evidences for mixing of different melts in the magma chamber. Amphibole phenocrysts are present in all rock types. The Tamara monogenetic cone with a basaltic composition is situated in several kilometers to the NW of Kizimen volcano. Some ol-cpx-plag-(amph) basalts and andesites from the Upper Pleistocene (~200 Ka) Tumrok ridge, which forms the basement of Kizimen, are sampled for comparison with the more Recent rocks.

Central Kamchatka depression (CKD)

Shiveluch, Kharchinsky and Zarechny volcanoes (NCKD)

These Upper Pleistocene to Holocene volcanoes are situated in the North of the Kamchatka river and form the northern termination of active volcanism on Kamchatka. Our samples are represented by ol-, cpx-, plag-, and occasionally amph-bearing Mg-basalts and -andesites. It was shown previously, that slab melts (adakites), related to the special plate tectonic environment in this area, are a substantial component in these rocks (Volynets et al., 1997a). Despite these volcanoes are relatively far from our transect, we will use them to detect adakitic tendencies in the other rocks.

The Kluchevskoy group

The Kluchevskoy group includes 10 large stratovolcanoes and some hundred cinder cones. The famous Holocene Kluchevskoy volcano (~4800 m) is the largest volcano on Kamchatka and the most active arc volcano worldwide. It is composed of high-Mg to high-Al basalts and andesites, similar to the southern Tolbachik. The samples from Kluchevskoy were already discussed in (Dorendorf et al., 2000b). The Tolbachik samples are derived as well from the stratovolcano as from Holocene cinder cones, including the fissure eruption of 1975-76. The Ploskie Sopky volcano is a composite volcano with the older Krestovsky and Ushkovsky and the younger superimposed cone of basaltic to andesitic cinder cones. They contain ol, cpx and plag similar to the basalts from Kamen volcano. The other stratovolcanoes (Bezymianny, Zimina, Udina) are entirely composed of highly evolved andesitic to rhyodacitic rocks and therefore not suitable for this study.

Nikolka volcano

The Nikolka volcano is the most southern volcanic center of the CKD. It consists of Miocene to Early Pleistocene basalts and andesites. In sample 8864 amph occurs besides cpx and plag, all other samples contain mainly plag. The rocks are far from a primitive composition.

Sredinny ridge (SR)

Monogenetic cones at Achtang volcano (ACH) and around the village Esso (ESO)

Dozens of small monogenetic cones are situated in the distance of 160-200 km from the volcanic front, between Kluchevskaya Group of volcanoes and Ichinsky volcano. They are arranged on various faults parallel to the CKD. These cinder cones were formed during the Upper Pleistocene to Holocene intensification of volcanism in the Kamchatka region. Their basement consists of plateau basalts of Lower Pleistocene age. The cinder cones are formed by ol-cpx- and subaphyric basalts and basaltic andesites.

Ichinsky volcano (ICH)

Ichinsky volcano (3607m), the only active volcano of the SR, is located on the west flank of the Sredinny ridge. The basement of the modern volcano is built up by a Lower Quaternary shield volcano, which is composed of basaltic and andesitic plateau lavas, including olivine basalts. The modern cone of the Ichinsky stratovolcano was formed in the somma of the shield volcano. Upper Quaternary to Holocene andesitic, dacitic and rhyolithic flows and lava domes are widespread on the slopes. The mineralogy is variable from plag, cpx, opx in the more mafic to amph, qz and occasionally bt in the evolved rocks. Numerous Holocene cinder cones around the volcano are formed by olivine basalts and basaltic andesites. Previously studies (Volynets, 1994) have shown that they are represented by normal island arc basalts, as well as by intra-plate high-Ti basalts. We sampled rocks from the shield volcano, stratovolcano and cinder cones.

Tab.2-1 Major [wt.%] and trace elements [ppm] from the transect

	Gamchen																			
	GAM-02 Q4	GAM-06 Q3-4	GAM-07 Q3	GAM-08 Q3	GAM-12 Q4	GAM-14 Q4	GAM-16 Q3-4	GAM-18 Q4	GAM-19 Q2	GAM-20 Q2	GAM-20/2 Q2	GAM-21 Pliocene?	GAM-22 Pliocene?	GAM-23 Pliocene?	GAM-25 Q3	GAM-26 Q2	GAM-27 Q2	GAM-28 Q2	GAM-29 Q2	GAM-30 Q2
SiO2	57.50	56.80	51.60	52.30	54.70	55.80	54.90	56.40	55.30	55.90	55.80	53.70	52.80	54.30	61.50	50.60	58.90	49.80	58.80	51.60
TiO2	0.65	0.75	0.85	0.86	0.80	0.86	0.80	0.78	0.86	0.85	0.84	0.81	0.80	0.81	0.70	1.00	0.78	0.83	0.98	0.99
Al2O3	18.20	20.29	18.61	19.19	19.76	18.51	18.10	17.99	18.24	17.48	17.43	17.36	17.20	17.92	16.15	18.51	16.90	17.89	17.59	17.54
Fe2O3	5.27	1.33	3.43	2.26	2.30	3.38	2.59	2.68	2.70	1.95	1.91	2.36	2.49	2.71	2.00	2.87	2.23	2.59	2.86	3.43
FeO	2.09	4.52	5.73	6.64	4.67	5.39	5.79	5.71	5.95	6.16	6.16	7.08	6.88	6.09	3.78	8.48	4.62	7.96	4.80	7.71
MnO	0.16	0.13	0.18	0.18	0.14	0.18	0.17	0.17	0.17	0.17	0.17	0.19	0.19	0.17	0.13	0.20	0.14	0.20	0.20	0.20
MgO	2.95	1.67	5.35	4.39	2.98	3.62	4.23	3.65	4.14	4.58	4.61	5.58	5.95	4.66	2.52	4.94	3.27	6.24	2.49	5.17
CaO	7.32	8.22	9.12	9.77	8.44	7.96	8.44	7.61	8.09	8.46	8.44	9.31	9.54	9.09	5.71	9.93	6.60	10.93	6.31	9.13
Na2O	3.16	3.55	2.72	2.69	3.18	3.26	2.86	3.25	3.34	3.03	3.04	2.87	2.78	2.89	3.35	2.60	3.32	2.37	4.11	3.02
K2O	0.78	1.01	0.49	0.49	0.68	0.33	0.85	0.48	0.61	0.89	0.88	0.57	0.54	0.67	1.60	0.61	1.19	0.66	1.12	0.68
P2O5	0.12	0.14	0.12	0.12	0.12	0.13	0.11	0.12	0.12	0.14	0.14	0.12	0.12	0.13	0.12	0.11	0.14	0.13	0.23	0.15
LOI	0.34	0.51	1.58	0.44	0.46	0.46	0.34	0.34	0.22	0.40	0.40	0.19	0.60	0.30	1.75	0.46	0.71	0.21	0.31	0.31
Total	98.54	98.90	99.78	99.33	98.23	99.87	99.18	99.19	99.73	100.00	99.81	100.13	99.88	99.74	99.30	100.32	98.80	99.80	99.81	99.93
Li			2.2			1.5							2.4			2.5		1.5		
Be			0.23			0.23							0.25			0.25		0.28		
Sc	22	21	28	30	21	25	32	23	30	28	31	34	34	27	22	35	23	41	21	34
V	140	112	230	249	173	248	238	194	233	235	235	274	269	255	151	359	166	313	80	314
Cr	12	10	38	43	10	4	52	8	14	59	63	40	87	35	15	26	30	79	5	35
Co	17	12	32	29	17	22	25	26	25	26	22	39	35	31	16	38	20	40	8	41
Ni	0	0	20	7	0	4	9	1	0	11	7	29	46	28	7	13		30	0	32
Zn	79	69	72	71	68	67	80	72	84	78	77	88	84	82	71	101	73	80	95	99
Ga	16	19	17	17	20	16	19	18	17	17	18	17	17	18	16	21	16	17	19	18
Rb			9			4							8			9		11		
Sr	275	296	278	289	293	263	257	248	284	264	265	257	257	272	232	268	238	331	299	261
Y			18			20							19			19		17		
Zr	80	97	61	60	80	62	81	67	77	94	94	73	73	80	137	61	120	54	107	75
Nb			1.0			0.6							1.1			0.9		0.9		
Cs			0.28			0.10							0.38			0.53		0.41		
Ba	260	299	154	164	214	117	270	162	182	254	266	172	199	196	385	205	332	327	353	227
La			3.91			2.82							4.20			3.61		4.38		
Ce			11.49			9.41							12.70			10.90		13.07		
Pr			1.67			1.51							1.78			1.54		1.95		
Nd			8.20			8.01							8.49			7.80		9.47		
Sm			2.50			2.58							2.56			2.44		2.72		
Eu			0.84			0.89							0.85			0.83		0.88		
Gd			2.64			2.84							2.69			2.67		2.69		
Tb			0.46			0.49							0.47			0.47		0.44		
Dy			2.95			3.23							3.06			3.05		2.79		
Ho			0.65			0.73							0.69			0.67		0.61		
Er			1.97			2.18							2.08			2.04		1.79		
Tm			0.28			0.32							0.31			0.30		0.26		
Yb			1.89			2.15							2.08			1.95		1.68		
Lu			0.29			0.34							0.32			0.30		0.26		
Hf			1.60			1.65							1.99			1.53		1.45		
Ta			0.08			0.06							0.07			0.08		0.07		
Tl			0.04			0.01							0.05			0.05		0.04		
Pb			2.18			0.98							1.78			1.83		1.68		
Th			0.57			0.21							0.59			0.48		0.58		
U			0.26			0.14							0.28			0.23		0.32		

Major [wt.%] and trace elements [ppm] from the transect

Shmidt			Komarov									Kizimen								
SHM-01 Q3-4	SHM-03 Q3-4	SHM-04 Q3-4	KOM-01 Q3	KOM-02/2 Q3	KOM-03 Q4	KOM-05 Q4	KOM-06 Q3	KOM-08 Q4	KOM-09 Q4	KOM-11/2 Q4	KOM-14 Q3	TAM-01 Q4	KIZ-01 Q4	KIZ-01/1 Q4	KIZ-02 Q4	KIZ-04 Q4	KIZ-05 Q4	KIZ-07 Q4	KIZ-07/1 Q4	KIZ-08 Q4
50.60	59.10	50.90	52.60	53.70	60.70	59.90	51.70	56.80	58.80	61.00	53.50	51.40	63.60	49.70	62.40	60.60	56.20	60.10	52.90	57.70
0.89	0.70	0.77	0.84	0.75	0.85	0.85	0.83	0.92	0.86	0.82	0.81	0.83	0.58	1.22	0.65	0.66	0.88	0.77	1.10	0.93
16.17	18.44	18.13	17.15	16.00	16.86	17.01	16.32	17.14	17.01	16.48	17.84	15.76	16.17	18.84	16.54	17.29	17.26	16.87	18.35	17.12
3.75	3.78	2.92	2.20	1.86	1.79	1.81	2.03	3.99	2.45	2.19	3.19	9.37	2.41	5.31	2.69	2.75	3.43	3.83	4.22	3.63
5.94	3.49	6.44	7.01	6.48	5.01	5.22	7.47	4.32	4.77	4.43	6.24	0.43	3.03	5.56	3.21	2.53	4.75	3.09	5.30	4.19
0.18	0.21	0.18	0.18	0.17	0.14	0.15	0.18	0.17	0.14	0.14	0.18	0.19	0.13	0.19	0.14	0.13	0.17	0.15	0.19	0.17
8.07	2.21	6.91	6.39	7.33	3.08	3.19	8.20	3.66	3.45	2.82	5.36	8.43	2.44	5.20	2.67	2.65	3.99	3.10	4.41	3.58
10.39	6.99	10.39	9.66	9.36	6.63	6.82	9.68	7.21	7.01	6.24	9.33	9.23	5.34	9.25	5.89	5.63	7.17	6.34	8.48	7.07
2.34	3.60	2.50	2.58	2.55	3.30	3.30	2.41	3.03	3.25	3.42	2.83	2.72	3.69	2.74	3.73	3.61	3.27	3.58	3.26	3.44
0.57	0.46	0.57	0.79	0.80	1.35	1.28	0.68	1.03	1.17	1.40	0.56	0.73	1.66	0.76	1.57	1.48	1.14	1.46	0.89	1.25
0.12	0.06	0.11	0.13	0.12	0.14	0.13	0.11	0.13	0.13	0.14	0.12	0.23	0.16	0.17	0.15	0.19	0.16	0.16	0.19	0.18
0.45	0.96	0.55	0.41	0.70	0.55	0.41	0.56	1.51	0.34	0.32	0.36	0.66	0.61	0.73	0.40	2.19	1.17	0.38	0.50	0.57
99.47	100.00	100.37	99.94	99.83	100.39	100.07	100.17	99.90	99.38	99.40	100.31	99.98	99.82	99.67	100.04	99.70	99.59	99.83	99.79	99.82
9.6	7.7	6.1	7.1	6.8			5.2				7.9	7.9	16.3	14.2			10.2			
0.41	0.39	0.37	0.34	0.34			0.32				0.29	0.51	0.79	0.52			0.63			
36	18	34	33	35	23	26	37	26	24	20	30	31	15	26	17	15	21	18	26	24
257	34	285	274	246	197	210	267	244	205	171	269	221	114	300	137	146	208	163	250	199
335	0	117	137	309	22	24	368	11	20	16	11	481	17	15	16	26	10	12	11	19
43	7	37	36	33	17	17	41	20	18	21	36	36	14	30	18	14	29	17	26	21
103	0	54	35	89	0		119	0	3	0	24	166	0	2		1	7	0	0	0
78	50	81	79	75	73	74	81	81	78	72	84	79	55	79	61	57	68	63	74	65
15	16	18	15	15	16	16	16	18	17	17	17	15	16	17	16	15	17	15	18	16
15	7	12	18	15			13				9	15	38	14			26			
215	408	287	231	219	241	249	240	253	246	235	247	380	319	370	328	318	330	320	368	325
21	17	19	24	27			18				21	16	16	21			20			
74	62	60	84	86	140	132	74	106	127	147	71	86	121	86	124	115	102	117	96	117
1.6	1.1	1.4	1.5	2.0			1.1				1.7	2.4	4.2	2.9			3.5			
0.67	0.37	0.56	0.78	0.96			0.59				0.55	0.50	1.50	0.52			0.47			
189	168	241	261	234	359	364	226	286	340	366	174	358	676	310	593	608	458	567	376	451
3.68	3.99	5.52	4.36	3.83			3.94				4.54	7.62	10.16	5.85			7.73			
9.72	11.38	13.50	11.75	9.79			9.91				10.41	19.02	22.39	15.18			19.37			
1.57	1.79	1.92	1.87	1.69			1.63				1.40	2.69	3.32	2.34			2.76			
8.65	8.85	9.75	10.37	10.86			8.72				8.98	13.10	13.54	11.99			12.79			
2.51	2.80	3.10	2.89	2.53			2.47				2.78	3.72	2.89	3.36			3.23			
0.78	1.00	0.99	0.84	0.72			0.74				0.83	1.11	0.95	1.14			1.04			
2.67	2.55	2.90	3.14	3.01			2.61				2.88	3.29	2.58	3.28			2.97			
0.47	0.50	0.59	0.47	0.42			0.41				0.49	0.52	0.36	0.54			0.44			
2.85	3.20	3.35	3.23	2.79			2.78				2.98	3.38	2.28	3.33			2.94			
0.67	0.63	0.62	0.69	0.62			0.61				0.62	0.67	0.55	0.74			0.65			
2.18	1.86	1.93	2.13	2.00			1.79				2.12	2.06	1.46	2.18			1.85			
0.31	0.30	0.36	0.33	0.31			0.28				0.32	0.32	0.20	0.30			0.26			
1.90	2.18	2.35	2.00	1.80			1.70				2.02	2.05	1.39	2.00			1.72			
0.27	0.31	0.28	0.32	0.30			0.28				0.30	0.31	0.24	0.29			0.28			
1.91	1.52	1.73	2.19	2.11			1.75				1.93	2.27	1.91	1.99			1.88			
0.10	0.09	0.09	0.09	0.07			0.06				0.08	0.19	0.21	0.17			0.17			
0.02	0.03	0.04	0.08	0.11			0.06				0.08	0.03	0.27	0.10			0.10			
1.63	2.36	2.33	2.42	2.08			1.91				1.75	2.15	5.30	1.95			3.01			
0.57	0.28	0.61	0.82	0.84			0.82				0.52	0.91	3.19	1.02			1.42			
0.29	0.18	0.44	0.36	0.42			0.33				0.27	0.45	1.45	0.49			0.79			

Major [wt.%] and trace elements [ppm] from the transect

Kizimen										Ploskie Sopky				Ploskie Sopky high-K							
KIZ-09	KIZ-11	KIZ-17/2	KIZ-18	KIZ-19	KIZ-21	KIZ-22	KIZ-23	KIZ-24	KIZ-24/1	2330	2377	3-90	PLO-16	3-84I	5-90	2373	1-90	2032	2042A	306-84	128
Q4	Q4	Q3	Q4	Q3	Q3	Q3	Q4	Q4	Q4	Q3	Q3	Q4	Q3	Q3-4	Q4	Q3-4	Q3	Q3-4	Q3-4	Q4	Q4
63.30	55.70	57.30	61.60	50.30	55.40	61.30	63.60	54.70	51.60	50.41	51.63	50.10	58.20	58.28	56.72	54.18	49.95	55.13	53.06	51.60	50.86
0.61	0.97	0.84	0.67	1.20	1.07	0.64	0.58	1.03	1.28	0.99	1.73	0.86	1.19	1.37	1.41	1.63	0.97	1.74	1.08	1.66	1.24
16.10	17.61	17.19	16.50	16.50	17.22	16.54	16.14	17.44	17.91	15.27	16.67	15.79	18.54	16.32	16.27	16.40	17.09	16.65	17.27	16.93	15.01
2.41	2.90	2.76	2.46	2.97	3.14	3.08	2.60	3.07	4.29	3.47	2.35	3.00	1.78	1.89	2.39	2.96	3.32	2.46	1.99	2.18	2.20
3.10	5.52	4.84	3.52	8.01	4.96	2.91	2.74	5.49	5.78	6.64	8.02	6.68	4.58	5.81	6.20	6.58	6.70	6.72	6.41	7.82	7.39
0.13	0.17	0.17	0.14	0.21	0.18	0.13	0.13	0.17	0.19	0.19	0.17	0.17	0.11	0.17	0.18	0.16	0.17	0.15	0.15	0.16	0.17
2.41	4.16	4.14	2.72	5.22	3.05	2.86	2.37	4.16	4.42	7.97	4.99	7.84	1.76	2.53	2.95	3.48	6.88	3.55	4.97	4.70	8.05
5.42	7.70	7.24	5.84	9.59	7.36	5.71	5.32	8.18	9.13	10.30	8.13	10.26	6.82	5.54	6.15	6.63	10.52	7.01	8.23	8.00	9.94
3.74	3.30	3.33	3.76	2.70	3.66	3.51	3.69	3.18	3.03	2.59	3.42	2.57	3.84	4.51	4.34	3.60	2.66	3.58	3.28	3.41	2.80
1.72	1.14	1.28	1.52	0.71	1.37	1.40	1.66	1.10	0.87	0.87	1.84	0.99	2.54	2.48	2.23	2.07	0.87	2.22	1.44	2.05	1.36
0.15	0.17	0.18	0.15	0.21	0.26	0.16	0.15	0.17	0.19	0.22	0.53	0.22	0.67	0.54	0.49	0.58	0.18	0.65	0.35	0.59	0.36
0.42	0.33	0.33	0.71	1.87	1.78	1.15	0.61	0.47	0.85	0.67	0.62	0.65	0.49	0.69	0.49	1.05	0.41	0.70	0.84	0.69	0.57
99.52	99.67	99.60	99.58	99.48	99.46	99.39	99.60	99.16	99.53	99.58	100.10	99.13	100.52	100.12	99.82	99.33	99.72	100.56	99.07	99.80	99.93
				3.8				8.5	11.7	7.4		7.1			18.4		7.0			14.6	9.6
				0.44				0.56	0.56	0.57		0.45			1.31		0.52			1.45	0.88
15	21	22	18	35	26	16	13	22	33	39	24	32	17	23	26	21	38	22	24	24	35
115	220	190	133	316	187	130	108	246	324	308	307	294	176	194	246	318	346	321	253	288	275
13	16	47	20	42	11	34	19	24	21	462	118	312	2	15	90	202	279	42	82	81	408
13	27	20	21	37	20	14	13	27	27	45	35	39	10	19	22	30	39	27	29	32	41
0	6	20	1	25	0	8	2	2	0	84	47	82	1	0	2	27	46	32	36	45	105
55	71	76	58	94	83	60	57	72	80	97	107	87	81	99	104	99	71	100	82	110	91
15	16	17	16	18	19	15	15	19	17	15	19	16	19	19	19	18	16	19	17	19	16
				9				21	16	15		18			43		15			55	34
304	332	359	324	276	299	341	320	328	335	363	354	450	354	365	374	379	478	378	364	352	319
				32				20	23	20		16			33		17			33	26
126	98	124	124	104	140	109	124	99	90	76	205	65	339	218	199	239	66	266	97	210	133
				4.1				3.1	3.2	1.6		1.0			4.1		1.3			5.7	3.4
				0.31				0.79	0.59	0.37		0.38			1.31		0.32			1.74	0.97
655	459	466	606	164	200	591	669	419	323	307	422	279	808	760	692	687	332	711	466	485	324
				6.49				6.52	7.02	6.73		6.49			16.50		6.60			18.00	11.37
				19.11				16.57	18.10	16.61		15.00			40.60		17.61			44.21	29.32
				2.73				2.83	2.59	2.72		2.29			6.31		2.75			6.69	4.54
				13.11				12.73	13.08	13.28		12.21			28.38		12.66			30.32	21.03
				3.86				3.25	3.91	3.75		3.25			7.09		3.55			7.26	5.37
				1.14				1.08	1.26	1.15		0.97			1.90		1.08			1.91	1.51
				4.04				3.12	3.53	3.56		3.11			6.30		3.22			6.37	4.82
				0.70				0.46	0.63	0.60		0.44			1.00		0.51			1.01	0.77
				4.37				3.08	3.88	3.58		2.70			5.79		2.96			5.80	4.58
				0.94				0.76	0.75	0.72		0.61			1.16		0.61			1.17	0.94
				2.89				1.97	2.23	2.09		1.64			3.38		1.77			3.37	2.61
				0.42				0.27	0.34	0.32		0.22			0.49		0.25			0.51	0.39
				2.77				1.72	2.38	2.02		1.57			3.20		1.55			3.24	2.54
				0.42				0.30	0.32	0.31		0.25			0.48		0.24			0.49	0.38
				2.80				2.10	2.17	2.08		1.59			4.78		1.82			4.93	3.34
				0.21				0.14	0.19	0.12		0.07			0.21		0.32			0.29	0.39
				0.05				0.09	0.10	0.04		0.06			0.11		0.05			0.08	0.08
				2.03				2.73	2.63	3.11		3.20			7.80		3.13			10.14	3.87
				0.59				1.57	0.91	0.52		0.74			1.85		0.98			2.15	1.63
				0.38				0.77	0.61	0.37		0.33			1.17		0.39			1.27	0.76

Major [wt.%] and trace elements [ppm] from the transect

Tolbachik						**Tolbachik high-K**								**Kamen**	
TOL-6/2/1	TOL-6/2/2	TOL-6/4	655	TOL-7/3	TOL-7/4	TOL-6/1	TOL-6/3	TOL-6/5	TOL-6/6	TOL-7/1	TOL-7/2	201	22--8	2310	2311
1975.00	1975.00	Q4	1975.00	Q4	Q4	1975.00	Q4	Q4	Q4	Q4	Q4	1941.00	1975.00	Q4	Q1
51.40	51.20	49.80	50.46	53.34	51.36	52.10	50.90	51.70	51.40	50.69	51.73	50.21	51.10	50.54	51.83
0.96	0.96	1.04	0.95	1.10	1.11	1.69	1.22	1.43	1.15	1.69	1.42	1.18	1.59	1.12	0.96
13.79	13.76	13.53	13.42	17.41	16.13	17.21	14.57	15.25	14.51	16.62	18.18	14.17	17.51	16.83	17.16
3.67	3.34	3.18	2.14	8.66	9.09	3.59	3.59	3.28	3.64	10.06	8.58	3.60	2.25	3.05	3.36
5.86	6.06	6.84	7.16	9.62	10.11	6.30	6.31	7.10	6.09	11.18	9.54	6.46	7.20	6.81	5.69
0.18	0.18	0.19	0.17	0.17	0.18	0.17	0.18	0.18	0.18	0.17	0.16	0.17	0.16	0.18	0.16
9.52	10.03	10.71	9.67	5.05	6.79	4.67	9.10	7.19	8.86	4.65	3.62	9.61	4.34	7.13	6.39
11.71	11.65	11.58	11.60	8.58	9.43	8.14	10.19	9.21	10.29	8.18	8.89	9.83	8.30	10.32	9.43
2.34	2.44	2.26	2.37	3.32	3.07	3.47	2.73	2.93	2.54	3.55	3.50	2.61	3.46	2.74	3.12
0.88	0.86	0.79	0.85	1.17	1.04	2.07	1.29	1.54	1.15	1.86	1.87	1.26	1.97	0.57	0.68
0.20	0.20	0.20	0.21	0.25	0.23	0.60	0.35	0.44	0.32	0.54	0.51	0.34	0.56	0.15	0.16
0.39	0.41	0.38	0.63	0.00	0.00	0.43	0.36	0.50	0.60	0.00	0.00	0.47	0.79	0.58	0.70
100.90	101.08	100.50	99.63	99.05	98.42	100.42	100.78	100.76	100.73	97.99	98.44	99.91	99.22	100.03	99.64
			7.2									10.2	14.7	7.9	8.4
			0.59									0.90	1.41	0.40	0.42
42	39	39	38	27	32	25	36	31	41	23	23	33	22	38	32
263	272	292	270	272	280	286	276	302	283	306	274	271	270	318	262
391	421	483	418	63	167	60	438	218	430	60	48	569	165	231	225
46	47	52	40	26	35	30	41	38	41	35	29	47	30	32	33
117	143	174	99	26	62	48	177	90	158	55	27	168	45	33	44
80	78	85	75	90	86	107	89	98	85	106	93	87	99	82	81
16	16	15	16	19	19	20	16	17	16	20	20	16	19	17	16
			18									34	52	8	11
299	293	268	292	410	359	358	308	318	309	362	410	305	362	300	336
			19									27	32	22	20
82	81	79	79	101	101	215	130	162	119	202	178	124	199	70	77
			1.5									3.1	4.8	1.4	1.5
			0.46									0.91	1.58	0.22	0.35
232	215	212	229	370	309	489	322	389	303	445	462	296	467	168	240
			6.47									10.50	17.00	4.32	5.39
			16.33									27.03	41.87	11.95	14.02
			2.72									4.37	6.42	2.03	2.31
			13.59									20.14	29.03	10.72	11.38
			3.85									5.29	7.14	3.34	3.32
			1.12									1.46	1.84	1.10	1.05
			3.56									4.58	6.22	3.49	3.25
			0.58									0.75	0.97	0.64	0.56
			3.50									4.25	5.66	3.90	3.47
			0.72									0.84	1.17	0.83	0.71
			2.00									2.52	3.47	2.39	2.04
			0.29									0.37	0.49	0.35	0.31
			1.89									2.27	3.19	2.26	2.05
			0.28									0.34	0.48	0.34	0.31
			2.05									3.02	4.75	1.89	1.97
			0.08									0.14	0.28	0.17	0.14
			0.06									0.05	0.05	0.05	0.02
			2.03									3.23	7.49	2.19	2.44
			0.49									0.95	2.31	0.30	0.49
			0.32									0.65	1.26	0.26	0.33

Major [wt.%] and trace elements [ppm] from the transect

Kluchevskoy																**Nikolka**			
KLU-01	KLU-02	KLU-03	KLU-04	KLU-05	KLU-06	KLU-07	KLU-08	KLU-09	KLU-10	KLU-11	KLU-12	KLU-13	KLU-14	KLU-15	KLU-16	8864	8868	8878	8883I
Q4	Q4	Q4	Q4	Q4	Q4	Q4	Q4	Q4	Q4	Q4	Q4	Q4	Q4	Q4	Q4	Pliocene	Pliocene	Pliocene	Miocene
51.30	54.20	53.70	52.20	52.50	53.50	53.50	52.90	52.70	52.60	52.60	54.00	54.20	54.30	53.40	53.70	60.96	55.24	55.97	51.07
0.80	1.11	0.85	1.07	0.99	0.89	0.84	1.00	0.97	0.97	0.97	1.11	1.13	1.10	0.86	0.94	0.56	1.25	0.85	1.39
13.20	18.13	15.33	15.99	16.35	15.25	14.59	16.66	15.55	15.72	15.82	18.08	18.52	17.85	14.60	15.86	18.78	17.76	16.69	18.37
8.58	2.58	2.06	2.81	2.29	2.53	2.59	2.84	3.01	2.31	2.31	2.89	3.23	3.48	3.71	2.66	3.39	4.42	1.78	4.79
9.53	5.98	6.42	6.34	6.51	6.25	5.88	6.00	6.01	6.63	6.79	5.61	5.33	5.20	4.94	6.13	1.40	4.12	5.70	4.96
0.17	0.16	0.16	0.17	0.16	0.16	0.16	0.16	0.17	0.17	0.17	0.16	0.16	0.17	0.17	0.17	0.06	0.14	0.14	0.17
11.58	5.21	8.88	7.70	7.49	8.33	9.44	7.43	8.31	8.20	8.23	5.03	4.61	4.94	8.67	7.32	0.86	2.46	4.19	3.56
10.10	8.24	9.40	9.39	9.37	9.70	9.59	9.41	9.71	9.72	9.79	8.14	8.01	8.18	10.03	9.38	4.98	7.18	7.40	8.20
2.36	3.62	2.89	3.13	3.18	2.84	2.78	3.15	2.98	2.87	2.97	3.60	3.60	3.47	2.74	2.95	4.29	3.48	3.30	3.56
0.55	1.18	0.76	0.71	0.79	0.76	0.74	0.80	0.66	0.65	0.63	1.19	1.20	1.17	0.91	0.94	2.67	2.16	1.16	2.36
0.13	0.22	0.16	0.19	0.19	0.16	0.15	0.20	0.17	0.17	0.16	0.22	0.23	0.22	0.17	0.18	0.27	0.33	0.17	0.61
0.00	0.32	0.33	0.51	0.48	0.31	0.43	0.51	0.54	0.45	0.40	0.40	0.43	0.22	0.38	0.30	1.79	2.23	1.05	0.82
98.77	100.96	100.94	100.22	100.31	100.68	100.69	101.06	100.77	100.46	100.84	100.43	100.65	100.31	100.58	100.54	100.02	100.76	98.41	99.84
	13.2	8.3	7.8	9.1	8.1	8.6	8.9	8.3	7.5	7.9	13.9	13.3	13.5	9.8	10.9		19.2	5.0	15.5
	0.63	0.50	0.58	0.62	0.48	0.47	0.62	0.50	0.49	0.54	0.66	0.68	0.71	0.51	0.55		1.00	0.57	1.05
41	30	36	35	35	34	36	31	35	35	37	21	27	27	38	33	9	22	29	25
241	260	240	248	234	245	244	247	250	255	262	259	267	258	246	255	67	282	227	265
846	45	426	283	240	341	500	221	343	318	321	31	6	33	431	256	364	202	330	148
47	37	37	39	39	40	40	35	38	39	36	33	30	33	40	32	9	21	24	28
203	39	151	99	106	107	166	88	104	108	109	31	14	21	110	93	14	10	1	22
55	88	79	84	80	81	78	80	78	81	81	87	88	89	77	85	67	86	81	99
15	18	16	15	18	16	16	17	17	19	18	18	19	18	15	19	18	18	18	18
	18	12	10	12	11	12	12	10	9	9	19	19	19	16	15		46	19	41
243	393	324	293	315	299	312	319	290	290	287	397	403	374	333	341	476	419	416	469
	21	15	19	18	16	15	19	18	18	19	22	22	23	18	19		27	18	30
66	104	81	100	99	81	77	98	87	85	85	104	105	107	75	87	145	142	93	176
	1.8	1.2	1.7	1.7	1.2	1.3	1.8	1.4	1.5	1.4	2.0	1.9	2.0	1.3	1.5		3.0	1.7	4.4
	0.47	0.42	0.36	0.46	0.28	0.39	0.39	0.33	0.31	0.32	0.51	0.48	0.58	0.44	0.43		2.00	0.24	0.23
226	398	290	223	259	283	280	261	243	224	228	434	428	402	307	344	873	743	478	689
	7.55	5.41	6.12	6.69	5.03	5.31	6.72	5.54	5.32	5.36	8.43	8.20	8.42	6.80	6.09		14.38	8.12	20.60
	19.26	13.63	16.27	17.09	13.01	13.14	17.47	14.29	14.22	14.58	21.11	21.31	21.48	16.97	15.09		35.71	19.35	51.29
	3.16	2.17	2.62	2.77	2.14	2.13	2.83	2.38	2.34	2.46	3.39	3.54	3.61	2.71	2.49		5.28	2.98	7.66
	14.88	10.37	12.45	12.65	10.24	10.27	12.90	11.19	11.40	11.57	15.75	15.64	16.75	12.25	11.87		24.72	14.19	33.92
	4.07	2.94	3.54	3.41	2.91	2.99	3.50	3.07	3.21	3.25	4.14	4.11	4.27	3.36	3.35		6.33	3.67	7.65
	1.26	0.90	1.07	1.04	0.94	0.93	1.07	1.01	1.02	0.97	1.27	1.29	1.33	1.02	1.06		1.65	1.12	1.93
	3.75	2.89	3.52	3.35	3.01	2.87	3.35	3.18	3.20	3.20	3.77	3.76	3.88	3.04	3.32		5.41	3.26	6.16
	0.62	0.45	0.57	0.54	0.48	0.46	0.56	0.53	0.55	0.56	0.63	0.65	0.64	0.51	0.54		0.88	0.54	0.94
	3.82	2.87	3.66	3.27	3.07	2.91	3.46	3.36	3.42	3.42	3.84	3.82	4.04	3.05	3.42		4.90	3.14	5.33
	0.77	0.61	0.79	0.69	0.64	0.59	0.71	0.68	0.70	0.70	0.82	0.81	0.83	0.66	0.71		0.98	0.64	1.07
	2.22	1.68	2.27	1.98	1.82	1.73	2.06	1.95	2.06	2.04	2.36	2.34	2.38	1.84	1.99		2.85	1.83	3.05
	0.33	0.26	0.33	0.30	0.27	0.25	0.30	0.28	0.31	0.31	0.34	0.36	0.34	0.28	0.29		0.41	0.28	0.44
	2.13	1.61	2.10	1.91	1.67	1.61	1.98	1.84	1.98	1.96	2.15	2.16	2.26	1.69	1.94		2.64	1.71	2.86
	0.34	0.25	0.32	0.29	0.25	0.24	0.30	0.29	0.30	0.30	0.34	0.32	0.33	0.26	0.29		0.39	0.25	0.43
	2.49	1.88	2.35	2.25	1.98	1.86	2.32	2.08	2.07	2.03	2.55	2.56	2.57	1.89	2.04		4.02	2.51	4.38
	0.09	0.09	0.12	0.11	0.07	0.08	0.11	0.09	0.10	0.10	0.14	0.16	0.14	0.09	0.09		0.49	0.34	0.50
	0.06	0.05	0.03	0.05	0.03	0.05	0.04	0.03	0.03	0.04	0.07	0.06	0.05	0.02	0.13		0.18	0.08	0.05
	3.26	3.06	2.70	3.07	2.74	2.79	2.82	2.73	2.39	2.26	3.39	3.36	3.53	2.79	3.04		6.50	3.72	7.19
	0.77	0.61	0.49	0.56	0.55	0.59	0.59	0.48	0.48	0.44	0.80	0.78	0.79	0.71	0.65		1.70	0.65	2.47
	0.49	0.41	0.33	0.40	0.40	0.40	0.38	0.34	0.32	0.31	0.49	0.46	0.49	0.39	0.42		1.23	0.51	1.38

Major [wt.%] and trace elements [ppm] from the transect

Kharchinsky		Shiveluch			Zarechny	Achtang			Cinder cones around Esso							
8837	8840	2569	2577	2585I	90093	ACH-01	ACH-02	ACH-03	ESO-01	ESO-03	ESO-04	ESO-06	ESO-08	ESO-09	ESO-10	ESO-11
Q3	Q3	Q4	Q4	Q4	Q3	Q4	Q4	Q4	Q4	Q1?	Q1?	Q4?	Q4	Q4	Q4	Q4
50.08	50.64	54.99	52.65	55.93	51.71	54.40	51.20	53.40	53.70	53.10	52.95	60.50	50.60	54.90	52.30	52.50
0.88	0.90	0.71	0.83	0.69	0.85	0.90	0.94	0.98	0.84	0.87	0.87	0.64	0.98	0.77	0.76	0.82
13.46	13.86	14.97	15.19	15.16	13.64	17.28	15.97	17.02	18.22	18.11	18.01	17.91	17.78	17.94	17.13	17.49
3.95	4.49	5.17	6.00	2.62	1.78	2.28	2.94	2.31	3.06	2.50	2.27	2.09	2.39	2.74	3.04	2.73
5.42	4.74	2.80	3.30	4.88	7.34	5.19	5.84	5.77	5.03	5.57	5.73	3.98	6.43	4.98	5.47	5.82
0.16	0.16	0.15	0.17	0.15	0.17	0.15	0.16	0.15	0.16	0.15	0.15	0.16	0.16	0.15	0.16	0.15
12.29	11.30	7.01	6.78	7.42	10.43	5.13	7.89	6.15	5.16	5.47	5.48	2.32	6.51	4.84	6.49	6.36
9.62	9.62	8.54	9.30	8.56	9.35	7.62	9.61	8.19	8.36	8.56	8.55	6.10	9.75	8.15	9.27	9.16
2.69	2.84	3.24	3.26	3.39	2.70	3.28	2.86	3.19	3.28	3.24	3.17	3.57	2.92	3.16	2.70	2.91
0.89	0.95	1.33	1.29	1.29	1.05	1.54	1.16	1.34	1.14	1.15	1.15	1.85	0.88	1.14	1.02	1.04
0.18	0.19	0.23	0.32	0.23	0.19	0.31	0.29	0.28	0.23	0.22	0.22	0.26	0.23	0.23	0.20	0.22
0.69	0.74	0.59	0.61	0.29	0.61	1.13	0.66	0.76	0.31	0.68	0.67	0.38	0.59	0.50	0.70	0.29
100.31	100.42	99.73	99.71	100.59	99.81	99.21	99.53	99.54	99.49	99.62	99.21	99.75	99.21	99.51	99.24	99.49
7.4	7.6	8.7	9.2	8.4	7.2	7.2	5.4	9.2	9.2		8.1		3.1			5.0
0.49	0.48	0.74	0.81	0.69	0.49	0.77	0.56	0.69	0.70		0.70		0.47			0.55
30	31	27	32	29	32	23	30	22	22	28	27	16	30	26	27	29
252	257	185	262	206	255	196	243	216	217	230	231	127	261	206	227	242
862	789	555	188	366	840	99	337	163	107	120	121	9	186	95	230	205
50	53	30	34	27	46	26	37	31	32	30	34	13	34	27	35	38
255	262	57	28	75	141	49	112	90	58	65	60	0	69	45	75	77
81	77	72	95	69	75	74	78	76	75	76	76	77	81	73	76	77
17	17	16	17	17	15	19	17	19	16	20	18	17	17	18	17	15
12	11	24	23	21	18	25	21	21	21		20		14			19
476	487	512	525	508	378	598	530	583	657	641	641	584	592	649	599	620
16	16	15	18	16	17	22	21	21	18		18		19			16
66	69	81	80	81	71	122	93	115	80	80	79	101	70	85	67	74
1.2	1.1	2.1	1.5	2.0	1.3	6.4	3.9	5.5	2.9		3.1		1.7			2.0
0.28	0.18	0.74	0.70	0.43	0.34	0.44	0.41	0.36	0.48		0.46		0.36			0.36
331	331	347	324	341	290	576	373	461	502	481	493	720	369	576	414	443
6.49	6.62	8.27	7.01	7.71	5.71	12.79	8.76	10.60	8.18		7.89		6.11			7.34
17.01	17.06	18.70	16.91	18.11	14.45	33.09	24.03	28.53	22.01		21.26		17.72			20.06
2.69	2.79	2.94	2.75	2.77	2.38	4.21	3.27	3.72	2.88		2.80		2.54			2.66
13.55	13.72	13.68	13.12	12.84	11.65	17.79	14.66	16.12	12.81		12.41		12.08			11.78
3.68	3.68	3.47	3.65	3.27	3.27	4.02	3.62	3.77	3.09		3.04		3.15			2.92
1.09	1.09	1.02	1.11	0.96	0.99	1.20	1.11	1.13	0.97		0.95		1.02			0.92
3.17	3.20	3.00	3.28	2.88	3.07	3.47	3.30	3.34	2.63		2.60		2.85			2.54
0.52	0.53	0.49	0.53	0.46	0.52	0.51	0.50	0.47	0.40		0.39		0.45			0.39
2.92	2.87	2.87	3.11	2.73	3.09	3.02	3.04	2.87	2.31		2.32		2.64			2.24
0.58	0.60	0.57	0.67	0.56	0.63	0.63	0.64	0.61	0.48		0.48		0.54			0.45
1.67	1.71	1.63	1.86	1.56	1.84	1.82	1.89	1.79	1.43		1.44		1.58			1.34
0.24	0.24	0.26	0.28	0.24	0.27	0.27	0.27	0.24	0.20		0.21		0.23			0.19
1.45	1.45	1.64	1.86	1.63	1.76	1.70	1.71	1.52	1.35		1.34		1.47			1.23
0.21	0.23	0.25	0.28	0.24	0.27	0.27	0.27	0.26	0.21		0.20		0.22			0.18
2.05	2.09	2.26	2.08	2.19	1.91	2.99	2.37	2.74	2.09		2.04		1.82			1.89
0.13	0.10	0.12	0.15	0.14	0.08	0.30	0.18	0.23	0.15		0.15		0.10			0.10
0.03	0.02	0.08	0.06	0.14	0.08	0.13	0.10	0.11	0.09		0.10		0.08			0.07
3.07	2.84	5.17	3.89	3.77	2.87	5.11	3.25	4.03	4.59		4.30		2.66			3.99
0.45	0.44	1.02	0.80	1.25	0.59	1.22	0.71	1.03	0.69		0.69		0.38			0.70
0.31	0.31	0.52	0.49	0.54	0.41	0.63	0.38	0.47	0.41		0.40		0.26			0.43

Major [wt.%] and trace elements [ppm] from the transect

Ichinsky

6250 Q4	ICH-71 Q4	ICH-19 Q4	ICH-21 Q4	6283 Q3-4	ICH-01 Q4	ICH-02 Q4	ICH-03 Q1	ICH-04 Q1	ICH-05 Q1	ICH-07 Q3?	ICH-08 Q3?	ICH-09 Q3?	ICH-10 Q3?	ICH-11 Q3?	ICH-13 Q3?	6334/1 Q3	ICH-16 Q2	ICH-21/2 Q4	ICH-22 Q4	ICH-24 Q3
51.99	53.40	50.40	54.90	49.53	56.50	54.90	53.10	50.40	47.40	49.00	48.70	48.00	47.80	49.80	52.70	59.10	68.50	54.20	64.30	64.00
0.85	0.95	0.89	0.88	1.64	1.21	1.19	1.43	1.75	1.85	1.79	1.69	1.44	1.80	2.06	1.52	0.80	0.32	0.88	0.58	0.62
14.70	17.64	20.21	17.68	16.66	16.96	16.74	17.29	18.60	16.81	16.59	16.48	16.33	16.42	17.44	17.32	16.98	15.20	17.69	15.94	16.16
3.01	4.02	3.11	2.67	9.51	3.81	2.02	2.17	2.92	3.87	3.51	7.33	6.14	3.77	8.84	2.46	1.66	0.90	2.61	1.71	1.69
5.62	4.57	5.08	4.74	0.89	4.16	5.87	5.98	6.46	6.44	6.43	2.62	3.95	6.52	1.92	5.80	4.76	0.84	4.74	2.72	2.80
0.16	0.16	0.14	0.15	0.16	0.14	0.15	0.15	0.17	0.17	0.17	0.16	0.16	0.17	0.18	0.15	0.12	0.13	0.15	0.10	0.10
8.41	5.12	4.88	5.05	6.76	3.26	4.80	4.90	4.46	7.38	7.19	7.35	9.17	8.64	4.54	4.52	3.29	0.26	4.57	2.16	2.17
10.07	8.74	9.77	7.63	8.75	6.60	7.44	7.35	7.54	9.83	8.57	9.30	9.36	8.51	7.38	7.37	6.37	0.79	7.61	4.51	4.64
2.66	3.38	3.17	3.74	3.76	4.15	3.73	3.93	4.31	3.57	3.80	3.40	3.19	3.43	4.12	4.02	3.86	5.22	3.74	4.02	4.05
1.46	1.85	1.05	1.89	1.38	1.81	1.49	2.03	1.69	1.22	1.46	1.44	1.06	1.38	1.99	2.23	1.89	5.19	1.89	2.54	2.41
0.23	0.28	0.25	0.32	0.49	0.54	0.48	0.49	0.70	0.47	0.59	0.48	0.36	0.51	0.67	0.50	0.34	0.07	0.32	0.19	0.20
0.63	0.38	0.40	0.85	0.60	0.47	0.60	0.47	0.42	0.35	0.30	0.40	0.38	0.38	0.45	0.29	1.11	1.71	0.85	0.52	0.53
99.79	100.49	99.34	100.48	100.14	99.60	99.41	99.28	99.44	99.36	99.40	99.35	99.53	99.33	99.39	98.87	100.27	99.13	99.24	99.30	99.38
6.6		7.1		9.8		11.5	12.8		5.6	7.3	5.1		6.2	8.0	17.5	12.3				
0.81		0.70		1.71		1.05	1.30		0.98	1.02	1.06		1.16	1.58	1.51	1.15				
32	26	25	27	27	20	23	21	19	27	24	27	27	24	20	20	13	8	23	15	12
243	268	219	190	241	212	194	200	183	262	241	239	211	235	215	195	164	8	195	108	110
346	65	33	55	247	0	74	61	0	129	174	206	210	187	5	47	51	6	54	32	16
39	30	30	28	38	21	26	26	26	45	40	41	46	46	29	26	19	0	24	8	15
92	39	45	56	94	0	30	39	0	68	110	98	211	184	11	36	25	0	49	18	14
73	78	74	323	95	87	92	80	80	85	86	87	80	85	84	80	82	53	77	55	56
16	18	20	17	18	18	18	18	20	19	18	20	16	18	19	20	18	17	16	15	17
25		18		19		20	31		17	21	24		19	26	37	33				
503	604	722	583	672	600	596	606	841	690	688	634	602	686	738	616	526	44	587	389	398
18		15		24		22	20		19	20	20		20	25	22	20				
95	117	93	186	152	193	177	198	170	145	164	154	122	147	215	208	173	406	188	176	173
3.7		3.6		13.2		8.2	18.7		17.2	16.4	0.3		15.3	27.2	21.9	7.0				
0.38		0.21		0.24		0.30	0.61		0.20	0.32	0.43		0.29	0.40	0.71	0.58				
443	534	454	922	469	650	583	542	468	317	419	431	285	403	494	549	659	715	916	725	667
9.03		8.22		17.04		19.14	23.53		18.93	20.76	18.71		17.01	27.43	20.69	18.93				
22.24		19.00		42.86		46.27	53.59		43.35	49.94	42.21		38.40	57.82	44.99	44.31				
3.30		2.86		5.94		6.43	6.95		5.82	6.67	5.72		5.34	7.48	6.39	5.80				
15.19		14.02		26.19		28.21	28.30		25.59	28.57	24.75		25.30	33.37	27.77	23.38				
3.82		3.55		6.07		6.27	6.45		6.42	6.70	5.65		5.58	7.56	5.58	4.96				
1.11		1.19		1.74		1.79	1.91		1.99	2.08	1.73		1.79	2.26	1.68	1.31				
3.31		3.12		5.10		5.36	5.38		5.31	5.57	4.67		5.02	6.53	5.23	4.06				
0.52		0.49		0.78		0.79	0.81		0.82	0.81	0.71		0.73	0.99	0.70	0.61				
3.10		2.79		4.40		4.69	4.86		4.68	4.94	3.95		4.07	5.53	4.15	3.50				
0.61		0.55		0.85		0.92	0.91		0.83	0.92	0.75		0.79	1.07	0.90	0.69				
1.73		1.61		2.36		2.62	2.42		2.18	2.33	1.99		2.20	2.92	2.53	2.02				
0.25		0.24		0.34		0.37	0.36		0.31	0.32	0.28		0.30	0.44	0.32	0.29				
1.67		1.48		2.13		2.48	2.42		1.99	2.18	1.82		1.83	2.73	2.08	1.93				
0.25		0.23		0.32		0.37	0.37		0.29	0.33	0.28		0.27	0.41	0.33	0.30				
2.50		2.28		3.54		4.26	4.71		3.49	3.70	1.76		3.44	5.03	4.79	4.17				
0.42		0.24		0.92		0.46	1.16		0.84	0.85	0.01		0.55	1.31	0.99	0.60				
0.13		0.04		0.02		0.09	0.12		0.05	0.04	0.73		0.03	0.01	0.04	0.17				
4.25		3.43		4.62		5.57	5.31		2.17	3.13	2.93		2.18	2.89	2.54	7.47				
1.45		0.76		1.40		1.53	2.67		1.65	1.68	2.11		1.63	2.89	3.24	2.45				
0.71		0.39		0.50		0.59	0.91		0.58	0.63	0.68		0.57	0.97	1.10	0.99				

Major [wt.%] and trace elements [ppm] from the transect

Ichinsky

ICH-25 Q4	ICH-28 Q3	ICH-29 Q3	ICH-30 Q1	ICH-31 Q4	ICH-32 Q4	ICH-33 Q4	ICH-36 Q4	ICH-38 Q4	ICH-40 Q3	ICH-41 Q3	ICH-42 Q3	ICH-43 Q3	ICH-46 Q3	ICH-47 Q3	ICH-47/2 Q3	ICH-48 Q3	ICH-49 Q3	ICH-49/2 Q3	ICH-50 Q3	ICH-52 Q1?
65.50	55.80	53.00	58.30	54.50	53.80	61.80	56.70	53.10	68.30	57.40	61.90	69.50	62.10	60.20	60.20	61.30	59.10	59.30	63.30	59.20
0.54	0.90	1.11	0.77	0.91	1.24	0.71	1.03	1.24	0.56	0.95	0.67	0.57	0.71	0.71	0.72	0.76	0.70	0.70	0.59	0.96
15.81	16.85	17.55	17.03	17.61	16.78	16.10	16.74	16.88	15.58	17.08	17.04	15.90	16.79	16.82	16.87	17.07	16.52	16.54	15.92	17.24
1.49	1.89	2.82	1.81	2.49	2.12	1.58	1.68	2.69	1.06	2.16	1.73	1.05	2.30	2.38	2.35	2.15	2.23	2.22	1.46	2.79
2.47	5.18	5.21	4.39	4.91	5.88	3.66	5.11	5.69	1.49	4.34	3.61	1.60	2.92	3.43	3.43	3.51	3.51	3.51	2.95	4.05
0.09	0.13	0.14	0.12	0.13	0.15	0.12	0.14	0.15	0.09	0.12	0.11	0.11	0.10	0.11	0.11	0.10	0.11	0.11	0.11	0.12
1.73	4.97	5.04	3.39	4.60	5.20	3.00	3.83	5.08	0.74	3.23	2.52	0.75	2.08	3.38	3.36	2.16	3.27	3.29	2.08	2.94
4.16	7.71	8.46	6.71	8.08	7.48	5.35	6.16	7.70	2.12	6.35	5.73	2.20	4.97	6.41	6.42	5.41	6.28	6.26	4.54	6.22
4.04	3.57	3.49	3.70	3.47	3.91	3.89	3.98	3.77	4.69	3.77	3.78	4.93	4.00	3.54	3.46	4.04	3.35	3.37	4.02	4.10
2.54	1.31	1.27	1.53	1.31	1.49	2.19	2.13	1.46	3.80	2.06	2.17	3.89	2.48	2.16	2.17	2.13	2.11	2.13	2.51	2.07
0.17	0.32	0.37	0.29	0.30	0.48	0.25	0.43	0.58	0.13	0.36	0.20	0.13	0.21	0.22	0.22	0.23	0.21	0.22	0.20	0.40
0.54	0.51	0.59	0.94	0.69	0.92	0.58	0.96	0.35	0.33	1.18	1.38	0.37	1.83	1.39	1.39	1.83	1.44	1.44	0.55	0.61
99.08	99.15	99.05	98.98	99.00	99.44	99.23	98.89	98.70	98.89	99.00	100.85	100.99	100.49	100.75	100.70	100.69	98.83	99.09	98.23	100.70
29.0	10.4	10.1	15.2	12.3	9.3	23.3			23.6				20.9				11.9			
1.11	0.93	0.79	0.82	0.86	1.14	1.11			1.58				1.00				0.95			
14	22	24	21	24	22	15	17	23	8	17	17	9	16	17	17	17	20	18	15	19
100	172	216	168	199	188	125	149	205	31	166	154	35	141	161	165	164	153	157	103	180
12	97	72	38	66	108	56	78	103	4	18	12	11	3	37	42	1	44	44	24	7
10	31	33	16	26	31	18	20	30	1	20	16	6	14	16	22	14	19	20	14	19
	77	64	29	62	74	31	38	67	0	32	8	0	6	36	28	1	32	39	13	12
52	74	87	71	79	92	65	72	96	55	71	60	55	61	62	61	63	62	62	57	78
17	18	17	17	18	19	18	17	18	16	18	16	15	18	16	18	17	17	16	16	19
49	20	20	23	22	23	41			83				51				43			
366	532	581	518	559	588	427	568	633	298	532	476	303	435	481	481	477	475	472	397	550
13	18	17	15	16	21	16			17				15				16			
174	157	138	148	128	169	170	178	184	259	169	152	262	150	146	147	154	143	144	175	164
6.2	6.0	6.8	4.8	5.6	10.6	6.8			12.2				5.1				5.2			
1.21	0.40	0.39	0.42	0.49	0.44	0.98			1.54				1.20				1.05			
696	469	440	556	449	472	646	636	583	969	658	725	1005	701	685	690	735	677	667	746	649
16.14	16.53	13.54	16.19	13.24	20.29	16.61			22.15				13.33				15.49			
34.01	36.40	34.35	36.96	28.72	46.57	34.35			47.61				29.14				30.55			
4.55	4.69	4.87	5.02	4.03	6.18	4.61			6.21				3.95				3.97			
17.10	20.71	20.81	19.96	19.06	27.25	19.38			24.19				16.71				17.97			
3.58	5.13	4.91	4.90	4.55	6.39	4.11			5.24				3.84				4.32			
0.98	1.43	1.48	1.40	1.29	1.81	1.12			1.34				1.06				1.14			
3.01	4.38	4.16	3.94	4.12	5.12	3.66			4.11				3.42				3.73			
0.45	0.73	0.61	0.65	0.62	0.83	0.55			0.60				0.50				0.60			
2.80	4.15	3.72	3.83	3.42	4.59	3.17			3.85				3.09				3.24			
0.58	0.78	0.74	0.71	0.67	0.85	0.69			0.77				0.62				0.64			
1.59	2.23	1.95	2.00	2.01	2.39	1.91			2.15				1.88				2.00			
0.24	0.36	0.27	0.31	0.30	0.37	0.29			0.31				0.26				0.30			
1.73	2.31	1.83	2.15	1.82	2.43	1.85			2.24				1.81				1.94			
0.28	0.31	0.29	0.33	0.26	0.35	0.29			0.37				0.28				0.27			
3.42	3.86	3.28	3.87	3.43	4.18	3.54			5.16				3.99				4.05			
0.45	0.39	0.32	0.29	0.27	0.51	0.40			0.84				0.40				0.30			
0.26	0.11	0.08	0.15	0.12	0.12	0.22			0.23				0.23				0.25			
8.09	5.91	4.10	6.55	4.79	5.23	7.17			11.94				7.41				7.40			
4.05	1.82	1.32	2.10	1.81	1.81	3.34			5.72				3.83				2.74			
1.75	0.84	0.50	0.92	0.77	0.79	1.57			2.31				1.92				1.53			

Major [wt.%] and trace elements [ppm] from the transect

Ichinsky

ICH-54 Q4	ICH-55 Q2	ICH-57 Q4	ICH-58 Q1?	ICH-59 Q2	ICH-60 Q2	ICH-61 Q2	ICH-62 Q2	ICH-64 Q4	ICH-66 Q4	ICH-67 Q3?	ICH-68/2 Q3?	ICH-69 Q4	ICH-72 Q4	ICH-73 Q4	OV6397 Q3?	OV6398 Q3?	OV6401 Q3?	OV6403 Q3?
55.60	61.10	57.70	57.50	60.60	61.60	67.40	66.30	67.40	58.00	57.50	61.90	50.50	57.10	49.80	53.70	54.90	70.40	60.50
0.96	0.86	1.09	1.09	0.68	0.62	0.54	0.51	0.53	1.09	1.16	0.66	1.48	1.11	1.54	1.45	1.16	0.13	0.78
18.11	16.92	17.17	17.15	17.22	16.96	15.86	15.34	15.68	17.21	17.17	16.77	16.83	17.38	16.79	18.04	17.42	13.50	16.94
2.22	1.77	2.48	3.24	2.56	2.55	1.40	1.01	1.35	3.13	2.28	2.00	5.41	2.41	3.85	3.03	5.26	0.85	1.59
4.77	3.79	4.97	4.26	3.48	2.92	2.16	2.35	2.23	4.43	4.75	3.37	4.17	4.80	5.67	4.92	3.18	1.24	4.27
0.13	0.13	0.14	0.13	0.16	0.15	0.11	0.08	0.09	0.14	0.13	0.11	0.17	0.13	0.17	0.14	0.16	0.13	0.11
4.22	2.42	3.21	3.21	2.63	2.22	1.45	1.40	1.54	3.22	3.78	2.98	6.94	3.93	7.51	3.67	4.39	0.14	2.58
7.92	5.12	6.49	6.50	5.82	5.31	3.31	3.39	3.56	6.52	6.16	6.00	8.92	7.01	8.66	7.63	7.23	0.39	5.81
3.73	4.17	4.04	4.05	4.17	4.29	4.51	4.07	4.37	4.11	4.25	3.69	3.69	3.79	3.74	4.33	3.96	4.29	3.93
1.74	2.65	1.98	1.97	2.38	2.51	3.13	3.05	3.03	1.98	2.28	2.13	1.33	1.79	1.55	1.73	1.61	4.10	1.82
0.38	0.31	0.49	0.49	0.29	0.29	0.18	0.17	0.17	0.49	0.47	0.21	0.59	0.37	0.56	0.66	0.48	0.02	0.31
1.00	1.02	0.87	0.91	0.52	0.97	0.69	2.80	0.60	0.31	0.33	0.61	0.36	0.90	0.36	0.64	0.69	5.00	1.22
100.78	100.26	100.63	100.50	100.51	100.39	100.74	100.46	100.56	100.62	100.25	100.42	100.39	100.71	100.20	99.93	100.43	100.19	99.86
12.2												8.1	16.8					
1.02												1.09	0.99					
22	19	21	20	13	12	7	11	11	22	20	17	28	23	26	14	21	5	14
179	128	206	202	145	120	75	78	85	211	143	150	245	184	231	187	190	5	141
48	16	13	5	23	21	20	10	16	13	67	27	163	49	208	30	67	56	189
26	16	20	26	17	13	10	10	10	19	22	18	40	19	37	22	26	0	17
41	11	11	7	12	6	11	1	2	12	53	29	113	38	157	21	51	0	22
80	66	82	84	68	65	55	49	50	84	79	60	93	75	88	91	96	65	69
20	18	17	20	18	19	16	15	17	20	20	18	20	18	20	20	19	18	18
32												19	25					
645	464	586	586	588	575	341	334	345	592	561	467	709	544	679	829	604	15	507
18												23	19					
163	196	168	165	129	132	208	188	189	166	223	153	164	176	175	214	199	222	188
7.0												13.7	9.6					
0.75												0.34	0.35					
575	734	613	612	766	810	843	810	809	620	681	703	501	559	474	640	614	53	626
16.92												20.25	16.42					
36.98												46.72	38.02					
4.93												6.45	5.56					
23.19												29.38	23.22					
5.15												6.64	4.92					
1.42												1.91	1.47					
4.41												5.47	4.46					
0.69												0.81	0.65					
3.69												4.61	3.88					
0.72												0.88	0.86					
2.12												2.46	2.26					
0.32												0.36	0.30					
2.02												2.32	2.01					
0.29												0.35	0.33					
4.00												3.85	4.03					
0.36												0.68	0.46					
0.13												0.02	0.12					
6.40												4.04	5.54					
2.58												1.53	2.22					
1.16												0.58	0.77					

Tab. 2-2 Sr-, Nd-, and Pb-isotope composition of selected rocks of the transect

	$^{87}Sr/^{86}Sr$	$^{143}Nd/^{144}Nd$	$^{206}Pb/^{204}Pb$	$^{207}Pb/^{204}Pb$	$^{208}Pb/^{204}Pb$
EVF					
GAM-12	0.70338	0.51299	18.316	15.508	38.138
GAM-28	0.70333	0.51302	18.335	15.510	38.070
SHM-01	0.70332	0.51308	18.306	15.495	37.960
SHM-04	0.70337	0.51302			
KOM-02	0.70346	0.51305			
KOM-06	0.70336	0.51303	18.343	15.528	38.159
KOM-11	0.70360	0.51300			
KIZ-01/1	0.70333	0.51303			
KIZ-24	0.70336	0.51307			
KIZ-24/1	0.70336	0.51306	18.320	15.502	38.033
CKD					
2330	0.70340	0.51308	18.242	15.474	37.885
3--90	0.70344	0.51308	18.267	15.508	38.015
5--90	0.70343	0.51308			
KLU-16	0.70358	0.51309			
2310	0.70350	0.51312	18.292	15.478	37.885
22--8	0.70339	0.51311			
655	0.70338	0.51307			
201	0.70336	0.51309	18.192	15.482	37.885
TOL-03	0.70334	0.51309	18.185	15.472	37.850
TOL-06	0.70334	0.51309	18.154	15.421	37.698
8883	0.70348	0.51310			
KLU-01	0.70353	0.51309	18.309	15.498	37.973
KLU-03	0.70357	0.51310	18.281	15.500	37.971
KLU-04	0.70353	0.51307	18.285	15.498	37.970
KLU-06	0.70355	0.51309			
KLU-07	0.70354	0.51307	18.297	15.496	37.972
KLU-08	0.70352	0.51308	18.295	15.517	38.010
KLU-09	0.70351	0.51311			
KLU-10	0.70349	0.51311	18.292	15.514	37.999
KLU-11	0.70350	0.51310	18.287	15.505	37.974
KLU-12	0.70366	0.51309	18.303	15.509	37.997
KLU-13	0.70366	0.51309			
KLU-14	0.70362	0.51309			
KLU-15	0.70355	0.51312	18.300	15.489	37.941
2569	0.70341	0.51313			
2585	0.70339	0.51311	18.357	15.483	37.918
8837	0.70346	0.51309			
90093	0.70336	0.51310			
SR					
ESO-04	0.70332	0.51308			
ESO-08	0.70335	0.51308	18.249	15.486	37.916
ACH-02	0.70335	0.51303			
ACH-03	0.70327	0.51305			
6250	0.70335	0.51307			
6283	0.70336	0.51302			
6334/1	0.70336	0.51305			
ICH-02	0.70337	0.51303			
ICH-05	0.70338	0.51297	18.057	15.476	37.952
ICH-07	0.70338	0.51309			
ICH-09					
ICH-10	0.70337	0.51297			
ICH-19	0.70331	0.51304	18.248	15.497	37.953
ICH-31	0.70335	0.51303	18.248	15.488	37.975
ICH-32	0.70337	0.51302			
ICH-49	0.70334	0.51307			
ICH-64	0.70329	0.51306			

Tab. 2-3 Results of U-Th isotope analyses on young volcanics of Kamchatka

Sample-No.	**U (ppm)**	**Th (ppm)**	**{230/232}**	**Error**	**(238/232)**	**Error**	**(238/230)**	**Error**
SHM-01	0.29	0.53	1.68	0.02	1.65	0.01	0.98	0.01
GAM-14	0.15	0.28	1.78	0.08	1.61	0.00	0.91	0.04
KIZ-24/1	0.56	0.98	1.84	0.02	1.72	0.01	0.94	0.01
KOM-09	0.78	1.95	1.27	0.01	1.22	0.01	0.96	0.01
KLU-01	0.41	0.66	1.81	0.02	1.88	0.01	1.04	0.01
KLU-03	0.44	0.63	1.95	0.00	2.12	0.01	1.08	0.00
KLU-08	0.41	0.61	1.92	0.03	2.06	0.01	1.07	0.01
KLU-10	0.33	0.46	2.10	0.02	2.18	0.01	1.04	0.01
KLU-13	0.51	0.77	1.86	0.02	2.01	0.01	1.08	0.01
KLU-14	0.52	0.80	1.92	0.01	1.95	0.01	1.01	0.01
KLU-15	0.40	0.68	1.79	0.01	1.79	0.01	1.00	0.01
3/90	0.39	0.63	1.79	0.02	1.86	0.01	1.04	0.01
5--90	1.27	2.02	1.90	0.02	1.90	0.01	1.00	0.01
2310	0.27	0.34	2.29	0.03	2.40	0.01	1.05	0.01
TOL-01	1.26	2.14	1.84	0.02	1.79	0.01	0.97	0.01
TOL-02/1	0.34	0.57	1.81	0.02	1.82	0.01	1.01	0.01
TOL-03	0.68	1.16	1.92	0.02	1.77	0.01	0.92	0.01
TOL-7/04	0.48	0.77	1.87	0.03	1.89	0.01	1.01	0.02
2585	0.55	0.96	1.61	0.02	1.75	0.01	1.09	0.02
BAK-04	0.35	0.70	1.61	0.02	1.50	0.01	0.93	0.00
ESO-08	0.29	0.46	1.90	0.03	1.92	0.01	1.01	0.02
ACH-01	0.65	1.34	1.54	0.01	1.48	0.01	0.96	0.01
ICH-02	0.59	1.47	1.36	0.02	1.22	0.01	0.89	0.01
ICH-33	1.36	3.33	1.33	0.01	1.24	0.01	0.93	0.01
ICH-64	2.34	4.48	1.44	0.02	1.58	0.01	1.10	0.01
ICH-69	0.60	1.57	1.19	0.01	1.15	0.01	0.97	0.01

References

Avdeiko, G.P., Volynets, O.N., Antonov, A.Y. and Tsvetkov, A.A., 1991. Kurile island-arc volcanism; structural and petrological aspects. In: L.P. Zonenshain (Editor), The achievements of plate tectonics in the USSR. Tectonophysics. Elsevier, Amsterdam, Netherlands, pp. 271-287.

Ayers, J., 1998. Trace element modeling of aqueous fluid - peridotite interaction in the mantle wedge of subduction zones. Contributions to Mineralogy and Petrology, 132: 390-404.

Ayers, J.C., Dittmer, S.K. and Layne, G.D., 1997. Partitioning of elements between peridotite and H_2O at 2.0-3.0 GPa and 900-1100 degrees C, and application to models of subduction zone processes. Earth and Planetary Science Letters, 150(3-4): 381-398.

Balesta, S.T., 1991. Earth crust structure and magma chambers of the areas of present Kamchatka volcanism. In: S.A. Fedotov and Y.P. Masurenkov (Editors), Active volcanoes of Kamchatka. Nauka, Moscow, pp. 36-45.

Baranov, B.V., Seliverstov, N.I., Murav, A.V. and Muzurov, E.L., 1991. The Komandorsky Basin as a product of spreading behind a transform plate boundary. In: L.P. Zonenshain (Editor), The achievements of plate tectonics in the USSR. Tectonophysics. Elsevier, Amsterdam, Netherlands, pp. 237-269.

Bebout, G.E., 1995. The impact of subduction-zone metamorphism on mantle-ocean chemical cycling. In: H. Staudigel, F. Albarede, D. Hilton and T. Elliott (Editors), The mantle-ocean connection. Chemical Geology. Elsevier, Amsterdam, Netherlands, pp. 191-218.

Bourdon, B., Wörner, G. and Zindler, A., 1999. U-Th evidence for crustal involvement in the petrogenesis of Nevados de Payachata, Chile. .

Bourdon, B., Zindler, A. and Woerner, G., 1994. Evolution of the Laacher See magma chamber; evidence from SIMS and TIMS measurements of U-Th disequilibria in minerals and glasses. Earth and Planetary Science Letters, 126(1-3): 75-90.

Brenan, J.M., Shaw, H.F., Ryerson, F.J. and Phinney, D.L., 1995. Mineral-aqueous fluid partitioning of trace elements at 900 degrees C and 2.0 GPa; constraints on the trace element chemistry of mantle and deep crustal fluids. Geochimica et Cosmochimica Acta, 59(16): 3331-3350.

Chabaux, F. and Allegre, C.J., 1994. ^{238}U- ^{230}Th- ^{226}Ra disequilibria in volcanics; a new insight into melting conditions. Earth and Planetary Science Letters, 126(1-3): 61-74.

Davidson, J.P., 1996. Deciphering mantle and crustal signatures in subduction zone magmatism. In: G.E. Bebout, D.W. Scholl, S.H. Kirby and J.P. Platt (Editors), Subduction top to bottom. Geophysical Monograph. American Geophysical Union, Washington, DC, United States, pp. 251-262.

Defant, M.J. and Drummond, M.S., 1990. Derivation of some modern arc magmas by melting of young subducted lithosphere. Nature (London), 347(6294): 662-665.

Dorendorf, F., Churikova, T., Koloskov, A. and Wörner, G., 2000a. Geochemical study of the Bakening volcano and surrounding monogenetic centers. (in prep.).

Dorendorf, F., Wiechert, U. and Wörner, G., 2000b. Hydrated sub-arc mantle: a source for Kluchevskoy volcano, Kamchatka/Russia. Earth and Planetary Science Letters, 175(1-4): 69-86.

Erlich, E.N. and Gorshkov, G.S., 1979. Quaternary volcanism and tectonics in Kamchatka. Bulletin Volcanologique, 42. Springer International [for the] International Association of Volcanology and Chemistry of the Earth's Interior (IAVCEI), Heidelberg, International, 298 pp.

Erlikh, E.N., Shantser, A.Y. and Kutyyev, F.S., 1971. Meymechity vostochnoy Kamchatki Translated Title: Meymechites of eastern Kamchatka. Izvestiya Akademii Nauk SSSR. Seriya Geologicheskaya, 2: 3-9.

Fedotov, S.A. and Masurenkov, Y.P., 1991. Active volcanoes of Kamchatka, Moscow.

Gill, J.B., 1981. Orogenic andesites and plate tectonics. Springer, Berlin, Federal Republic of Germany, 401 pp.

Gorbatov, A.V., 1997. Sismicidad y estructura de la zona de subduction de Kamchatka. Ph.D. Thesis, Mexico, Mexico, 144 pp.

Gorelchik, V.I., Shirokov, V.A., Firstov, P.P. and Chubarova, O.S., 1997. Shiveluch Volcano; seismicity, deep structure and forecasting eruptions (Kamchatka). Journal of Volcanology and Geothermal Research, 78(1-2): 121-137.

Hawkesworth, C.J., Gallagher, K., Hergt, J.M. and McDermott, F., 1993. Mantle and slab contributions in arc magmas. Annual Review of Earth and Planetary Sciences, 21: 175-204.

Hawkesworth, C.J., Turner, S.P., McDermott, F., Peate, D.W. and van, C.P., 1997. U-Th isotopes in arc magmas; implications for element transfer from the subducted crust. Science, 276(5312): 551-555.

Heuser, A., Simon, K., Wörner, G. and Dorendorf, F., 2000. Chalkophile elements in mafic volcanites of Kamchatka. (in prep.).

Hochstaedter, A.G., Kepezhinskas, P., Defant, M., Drummond, M. and Koloskov, A., 1996. Insights into the volcanic arc mantle wedge from magnesian lavas from the Kamchatka Arc. Journal of Geophysical Research, B, Solid Earth and Planets, 101(1): 697-712.

Hofmann, A.W., 1988. Chemical differentiation of the Earth; the relationship between mantle, continental crust, and oceanic crust. In: E. Welin (Editor), Isotope geochemistry; the Crafoord symposium. Earth and Planetary Science Letters. Elsevier, Amsterdam, Netherlands, pp. 297-314.

Kepezhinskas, P. et al., 1997. Trace element and Sr-Nd-Pb isotopic constraints on a three-component model of Kamchatka Arc petrogenesis. Geochimica et Cosmochimica Acta, 61(3): 577-600.

Kersting, A.B. and Arculus, R.J., 1995. Pb isotope composition of Klyuchevskoy Volcano, Kamchatka and North Pacific sediments; implications for magma genesis and crustal recycling in the Kamchatkan arc. Earth and Planetary Science Letters, 136(3-4): 133-148.

Koloskov, A.V., Volynets, O.N., Puzankov, M.Y. and Dorendorf, F., 2000. The first data on isotopic composition of minerals of ultramafic xenoliths from island arc type basalts (Avachinsky and Shiveluch volcanoes on Kamchatka). (in prep).

McCulloch, M.T. and Gamble, A.J., 1991. Geochemical and geodynamical constraints on subduction zone magmatism. Earth and Planetary Science Letters, 102(3-4): 358-374.

Melekestsev, I.V., Ponomareva, V.V. and Volynets, O.N., 1995. Kizimen Volcano, Kamchatka; a future Mount St. Helens? Journal of Volcanology and Geothermal Research, 65(3-4): 205-226.

Miller, D.M., Goldstein, S.L. and Langmuir, C.H., 1994. Cerium/ lead and lead isotope ratios in arc magmas and the enrichment of lead in the continents. Nature (London), 368(6471): 514-520.

Molzahn, M., Reisberg, L. and Woerner, G., 1996. Os, Sr, Nd, Pb, O isotope and trace element data from the Ferrar flood basalts, Antarctica; evidence for an enriched subcontinental lithospheric source. Earth and Planetary Science Letters, 144(3-4): 529-545.

Navon, O. and Stolper, E., 1987. Geochemical consequences of melt percolation; the upper mantle as a chromatographic column. Journal of Geology, 95(3): 285-307.

Noll, P.D., Jr., Newsom, H.E., Leeman, W.P. and Ryan, J.G., 1996. The role of hydrothermal fluids in the production of subduction zone magmas; evidence from siderophile and chalkophile trace elements and boron. Geochimica et Cosmochimica Acta, 60(4): 587-611.

Peacock, S.M., 1993. Large-scale hydration of the lithosphere above subducting slabs. In: J.L.R. Touret and A.B. Thompson (Editors), Fluid-rock interaction in the deeper continental lithosphere. Chemical Geology. Elsevier, Amsterdam, Netherlands, pp. 49-59.

Pearce, J.A., 1983. Role of the sub-continental lithosphere in magma genesis at active continental margins. In: C.J. Hawkesworth and M.J. Norry (Editors), Continental basalts and mantle xenoliths; papers prepared for a UK Volcanic Studies Group meeting at the University of Leicester. Shiva Publ., Nantwich, United Kingdom, pp. 230-249.

Pearce, J.A. and Parkinson, I.J., 1993. Trace element models for mantle melting; application to volcanic arc petrogenesis. In: H.M. Prichard, T. Alabaster, N.B.W. Harris and C.R. Neary (Editors), Magmatic processes and plate tectonics. Geological Society Special Publications. Geological Society of London, London, United Kingdom, pp. 373-403.

Plank, T. and Langmuir, C.H., 1988. An evaluation of the global variations in the major element chemistry of arc basalts. Earth and Planetary Science Letters, 90(4): 349-370.

Plank, T. and Langmuir, C.H., 1993. Tracing trace elements from sediment input to volcanic output at subduction zones. Nature (London), 362(6422): 739-743.

Schmidt, M.W. and Poli, S., 1998. Experimentally based water budgets for dehydrating slabs and consequences for arc magma generation. Earth and Planetary Science Letters, 163(1-4): 361-379.

Shibata, T. and Nakamura, E., 1997. Across-arc variations of isotope and trace element compositions from Quaternary basaltic volcanic rocks in northeastern Japan; implications for interaction between subducted oceanic slab and mantle wedge. Journal of Geophysical Research, B, Solid Earth and Planets, 102(4): 8051-8064.

Stalder, R., Foley, S.F., Brey, G.P. and Horn, I., 1998. Mineral-aqueous fluid partitioning of trace elements at 900 °C-1200 °C and 3.0 GPa to 5.7 GPa: new experimental data for garnet clinopyroxene and rutile and implications for mantle metasomatism. Geochimica et Cosmochimica Acta, 62(10): 1781-1801.

Stolper, E. and Newman, S., 1994. The role of water in the petrogenesis of Mariana Trough magmas. Earth and Planetary Science Letters, 121(3-4): 293-325.

Sun, S.S. and McDonough, W.F., 1989. Chemical and isotopic systematics of oceanic basalts; implications for mantle composition and processes. In: A.D. Saunders and M.J. Norry (Editors), Magmatism in the ocean basins. Geological Society Special Publications. Geological Society of London, London, United Kingdom, pp. 313-345.

Tatsumi, Y. and Eggins, S., 1995. Subduction zone magmatism. Frontiers in earth sciences. Blackwell Science, Cambridge, 211 pp.

Tatsumi, Y., Hamilton, D.L. and Nesbitt, R.W., 1986. Chemical characteristics of fluid phase released from a subducted lithosphere and origin of arc magmas; evidence from high-pressure experiments and natural rocks. In: I. Kushiro (Editor), M. Sakuyama and H. Fukuyama memorial volume. Journal of Volcanology and Geothermal Research. Elsevier, Amsterdam, Netherlands, pp. 293-309.

Tatsumi, Y., Kogiso, T. and Nohda, S., 1995. Formation of a third volcanic chain in Kamchatka; generation of unusual subduction-related magmas. Contributions to Mineralogy and Petrology, 120(2): 117-128.

Todt, W., Cliff, R.A., Hanser, A. and Hofmann, A.W., 1984. ^{202}Pb-^{205}Pb spike for Pb isotope analysis. Terra Cognita, 4: 209.

Tribuzio, R., Messiga, B., Vannucci, R. and Bottazzi, P., 1996. Rare earth element redistribution during high-pressure-low-temperature metamorphism in ophiolitic Fe-gabbros (Liguria, northwestern Italy); implications for light REE mobility in subduction zones. Geology (Boulder), 24(8): 711-714.

Tsvetkov, A.A., Gladkov, N.G. and Volynets, O.N., 1989. Problema subduktsii osadkov i izotop ^{10}Be v lavakh Kuril' skikh ostrovov i Kamchatki Translated Title: Problem of sediment subduction and ^{10}Be isotope in lavas of Kurile Islands and Kamchatka Peninsula. Doklady Akademii Nauk SSSR, 306(5): 1220-1225.

Turner, S., McDermott, F., Hawkesworth, C. and Kepezhinskas, P., 1998. A U-series study of lavas from Kamchatka and the Aleutians: constraints on source composition and melting processes. Contributions to Mineralogy and Petrology, 133(3): 217-234.

Vazheyevskaya, A.A. et al., 1990. Quaternary evolution of volcanic rock composition in the Gamchenskoy volcano-tectonic structure, eastern Kamchatka. Volcanology and Seismology, 10(2): 245-271.

Volynets, O. et al., 1997a. Variations in geochemistry and Sr-Nd isotopes in lavas from the Northern Volcanic Group, Kamchatka; evidence for distinct sources at a subducting transform system. In: Anonymous (Editor), AGU 1997 fall meeting. Eos, Transactions, American Geophysical Union. American Geophysical Union, Washington, DC, United States, pp. 804.

Volynets, O.N., 1994. Geochemical types, petrology, and genesis of late Cenozoic volcanic rocks from the Kurile-Kamchatka island-arc system. International Geology Review, 36(4): 373-405.

Volynets, O.N., Karpenko, S.F., Kay, R.W. and Gorring, M., 1997b. Isotopic composition of Late Neogene K-Na alkaline basalts of Eastern Kamchatka: Indikators of the heterogeneity of the mantle magma sources. Geochemistry International, 35: 884-896.

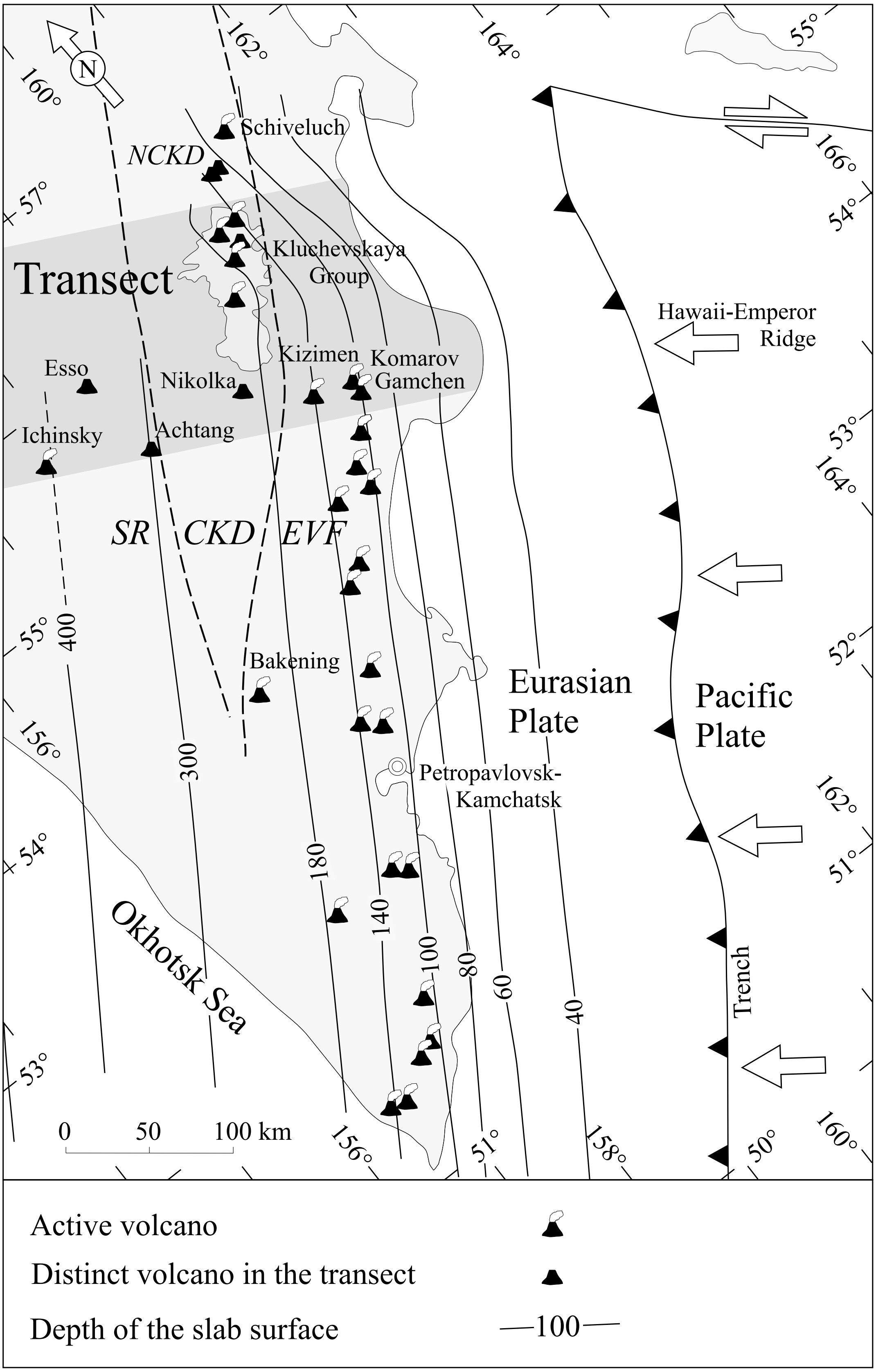

Fig. 2-1
General plate tectonic position of the Kamchatka arc (Erlich and Gorshkov, 1979; Gorbatov, 1997) and the location of the transect in N-Kamchatka.

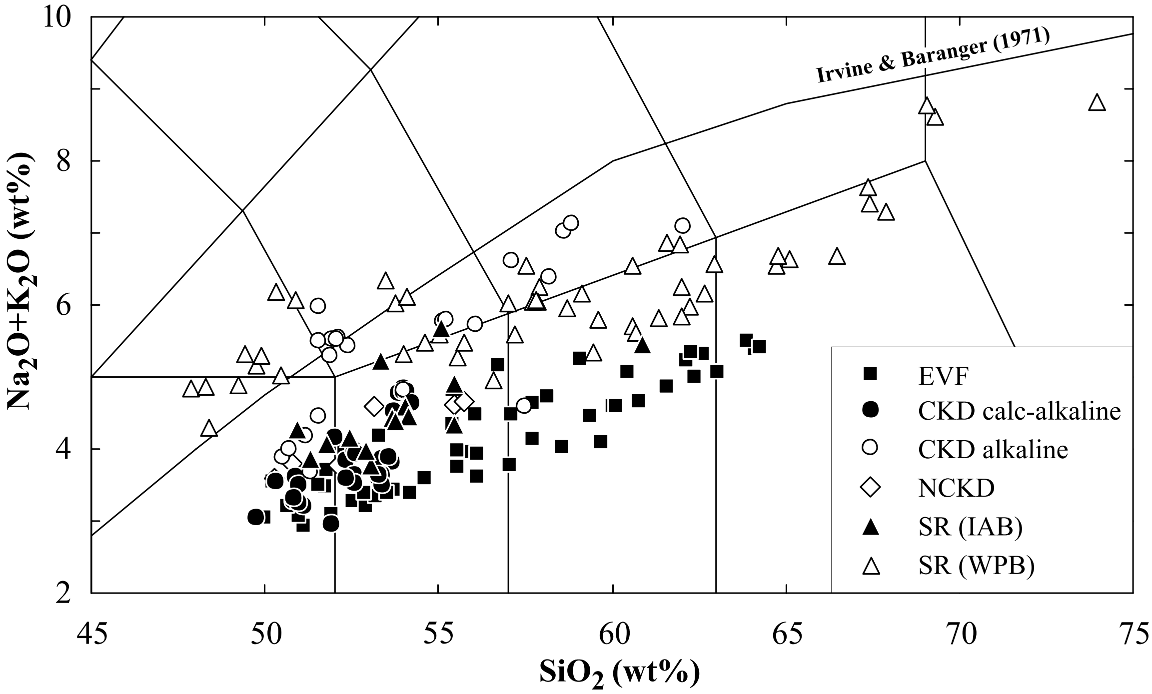

Fig. 2-2
(K_2O + Na_2O) vs. SiO_2 for volcanic rocks along the East - West transect in the North of Kamchatka Peninsula. Some high-K calc-alkaline rocks occur in the Central Kamchatka Depression (CKD), which are marked separately. Also the mafic WPB of Ichinsky from the Sredinny ridge (SR) plot into the high-K field.

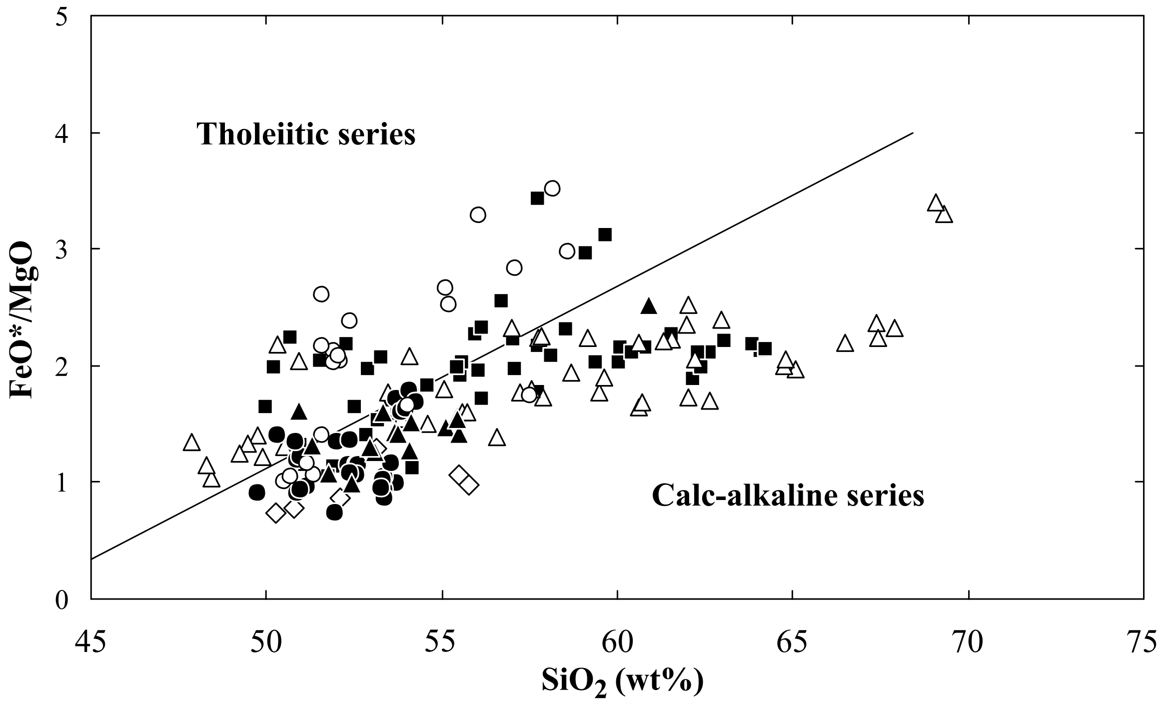

Fig. 2-3
Diagram of (FeO* / MgO) versus SiO_2. Most rocks of the EVF, CKD and SR follow the calc-alkaline trend. Only some rocks from the EVF and most of the high-K calc-alkaline rocks from the CKD plot into the tholeiitic field.

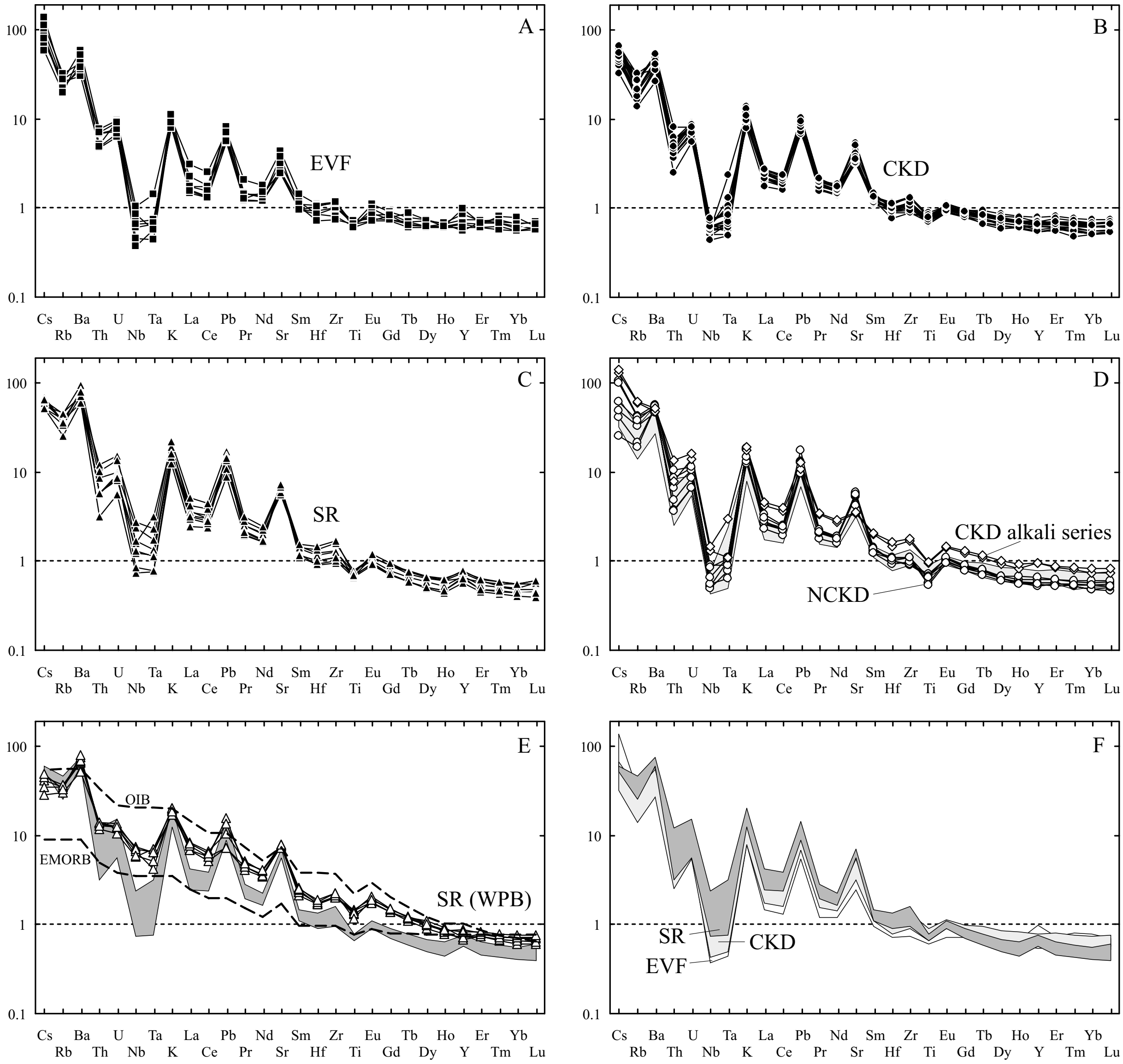

Fig. 2-4

Spider diagrams for mafic rocks with > 6 % MgO of the different regions of the North Kamchatka transect normalized on NMORB (Sun and McDonough, 1989). The order of incompatible elements is largely derived from Hofmann (1988) enlarged by Cs and all REE. Same symbols like in Fig. 2-2.

A-C) Trace element distributions in the EVF, CKD and SR.

D) High-K calc-alkaline rocks of the CKD and "adakitic" rocks of the NCKD compared with the typical island arc basalts of the CKD (shown by the gray field).

E) WPB compared with the "normal" island arc rocks of the SR (gray field) and the EMORB and OIB compositions after Sun and McDonough (1989).

F) Comparison of the pattern of typical arc basalts from each zone. For clarity, each zone is expressed by a compositional field.

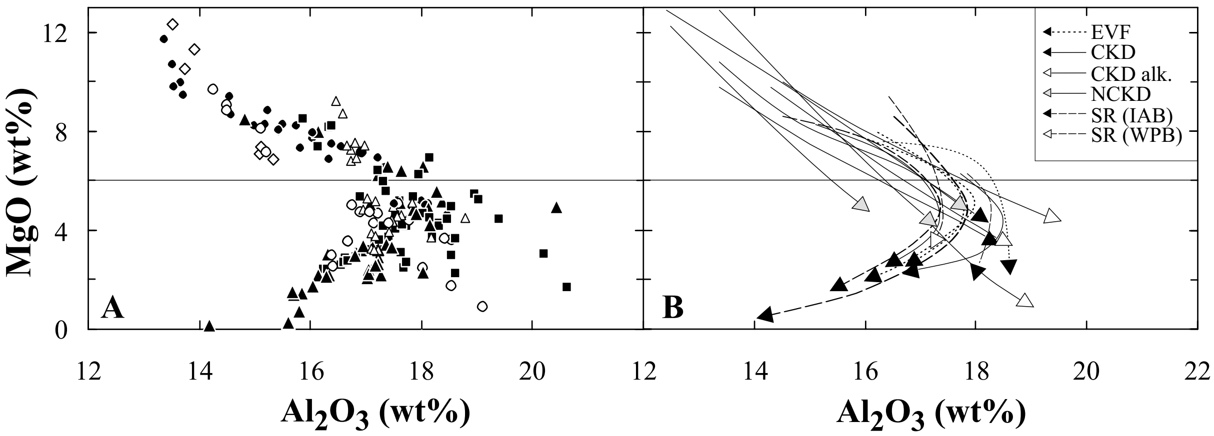

Fig. 2-5
A) MgO versus Al_2O_3 reflecting the beginning of plagioclase fractionation, which is connected with a strong decrease in Al_2O_3. Some outliers to higher Al_2O_3 are probably cumulates. Same symbols like in Fig. 2-2. For rocks with MgO > 6 % plagioclase fractionation can be regarded as negligible.
B) Similar diagram, which shows fractionation trends of single volcanoes, underlined by arrows. The EVF, CKD and SR are marked by dotted, solid and marked lines, respectively.

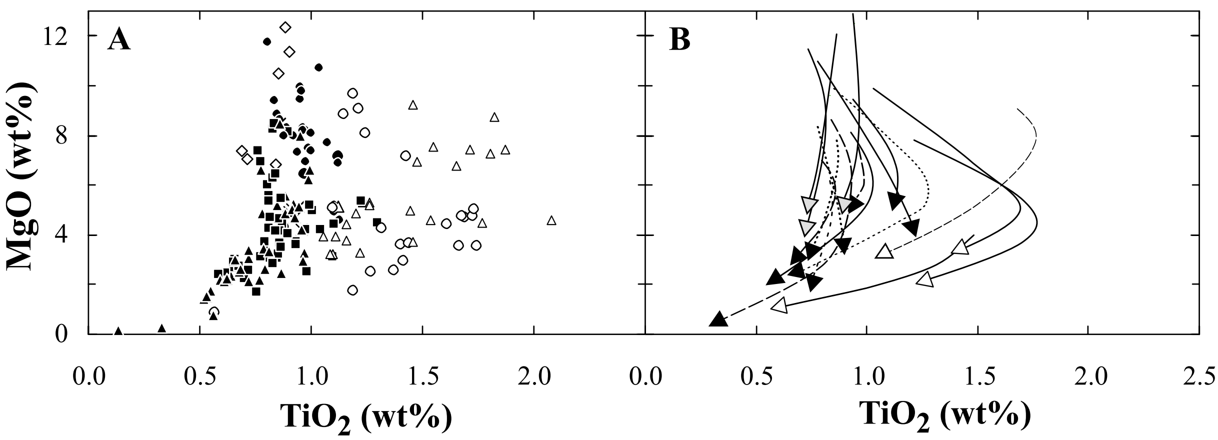

Fig. 2-6
A) MgO versus TiO_2, reflecting the extend of magnetite fractionation, which strongly decrease in TiO_2. In difference to MgO versus Al_2O_3 there is a larger scatter. Symbols derived from Fig. 2-2.
B) Fractionation trends, in space of MgO versus TiO_2 for single volcanoes, marked by arrows (lines like in Fig. 2-5). It is obviously that the large scatter is caused by a combination of source inhomogenities and the different beginning and extend of magnetite fractionation. The Ichinsky WPB are those with the highest TiO_2-concentrations, which probably fractionate magnetite from the very beginning.

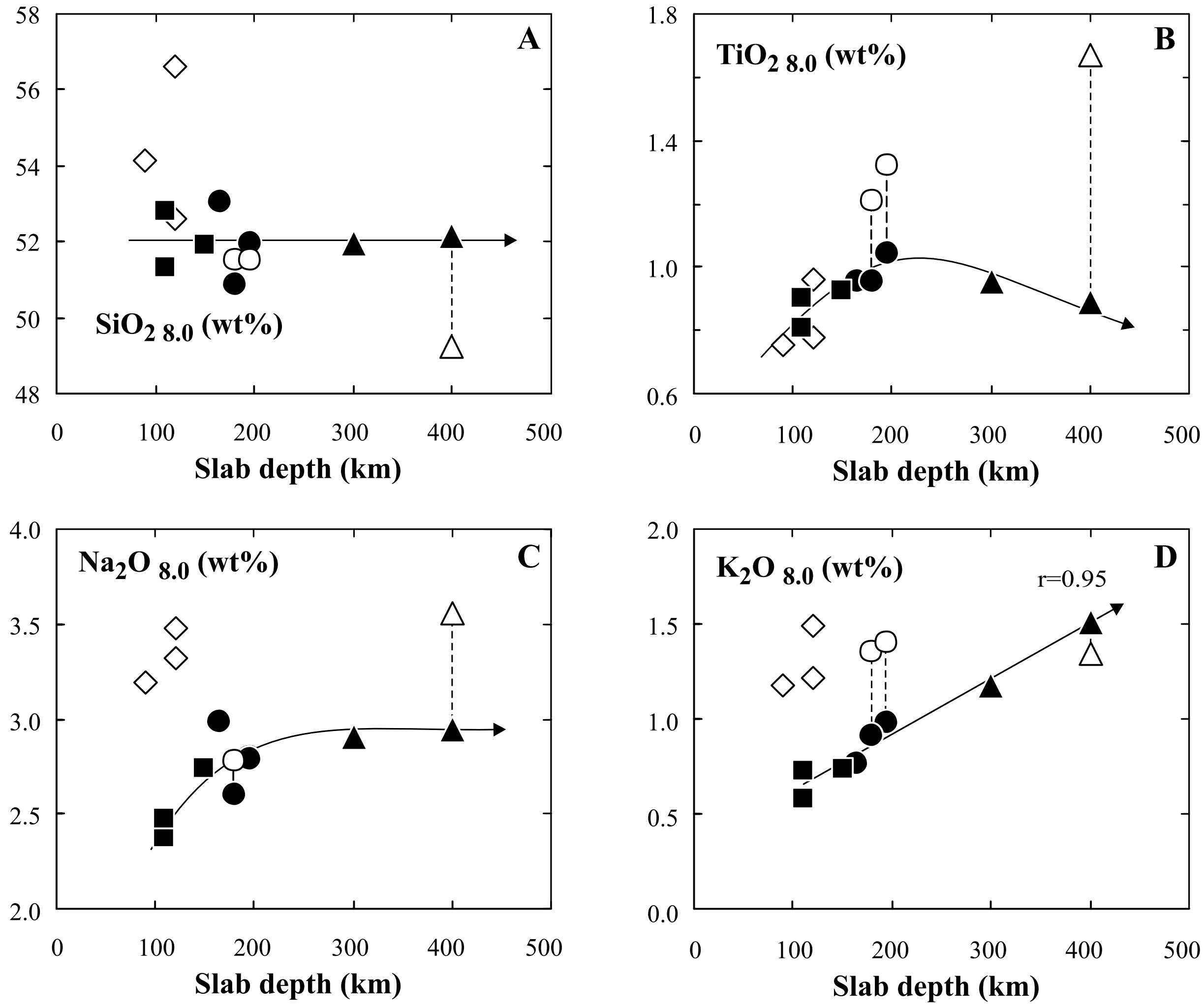

Fig. 2-7
A-D) On 8 % MgO normalized major element concentrations of single volcanoes in relation to the depth of the slab surface below the volcano. The typical arc series of Tolbachik, Ploskie Sopky and Ichinsky are connected by a dotted line with the high-K calc-alkaline series and WPB, respectively, occurring at the same volcano. For the linear trend of $(K_2O)_{8.0}$ the regression line and regression coefficient is shown additionally. The other lines were drawn just to underline the trends. Symbols like in Fig. 2-2.

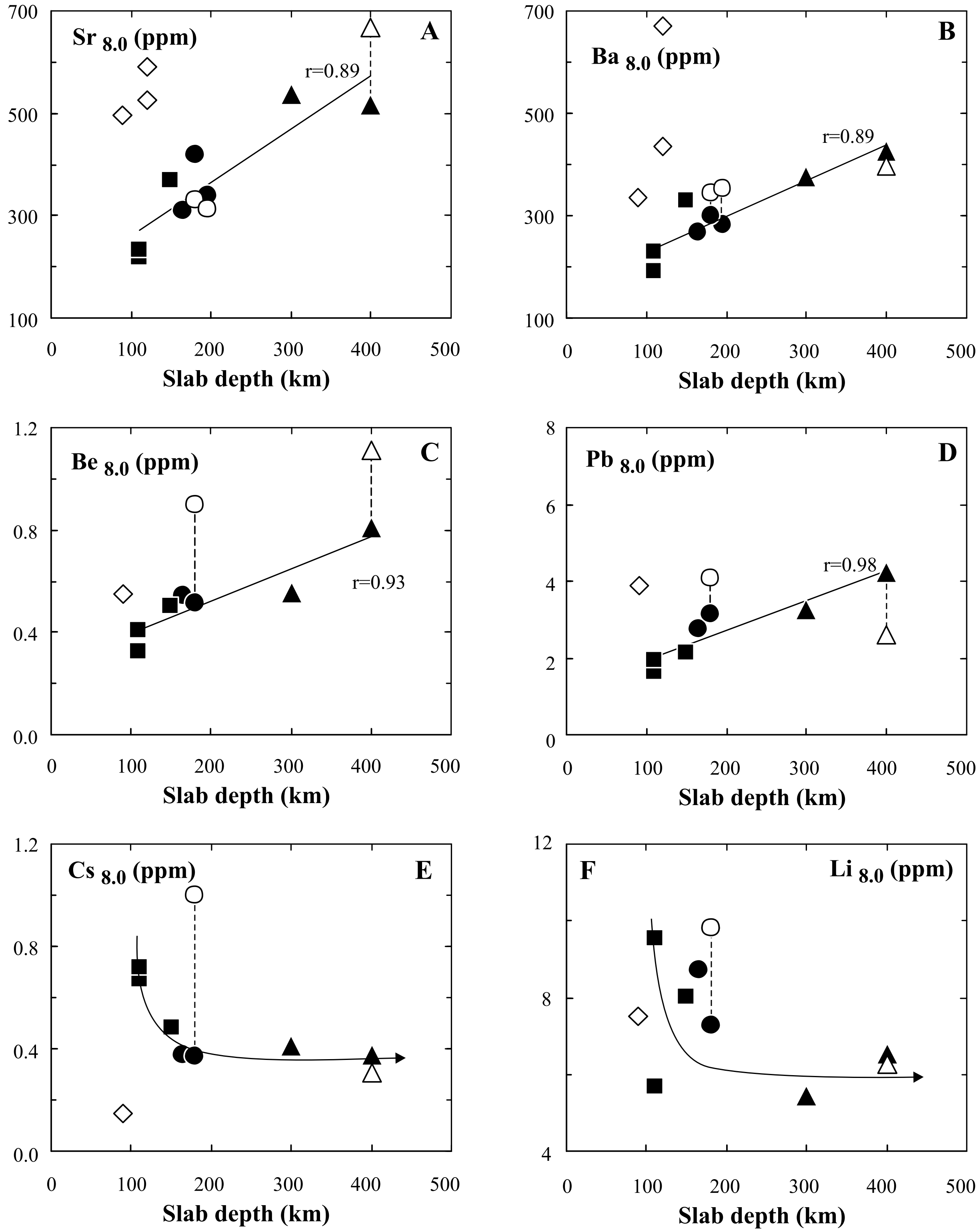

Fig. 2-8
A-F) On 8 % MgO normalized fluid mobile trace element concentrations of single volcanoes in relation to the depth of the slab surface below the volcano. There are well-defined linear trends of $Sr_{8.0}$, $Ba_{8.0}$, $Be_{8.0}$ and $Pb_{8.0}$, which are marked by regression lines. In difference $Cs_{8.0}$ and $Li_{8.0}$ strongly decrease from the EVF to the SR. Symbols derived from Fig. 2-2.

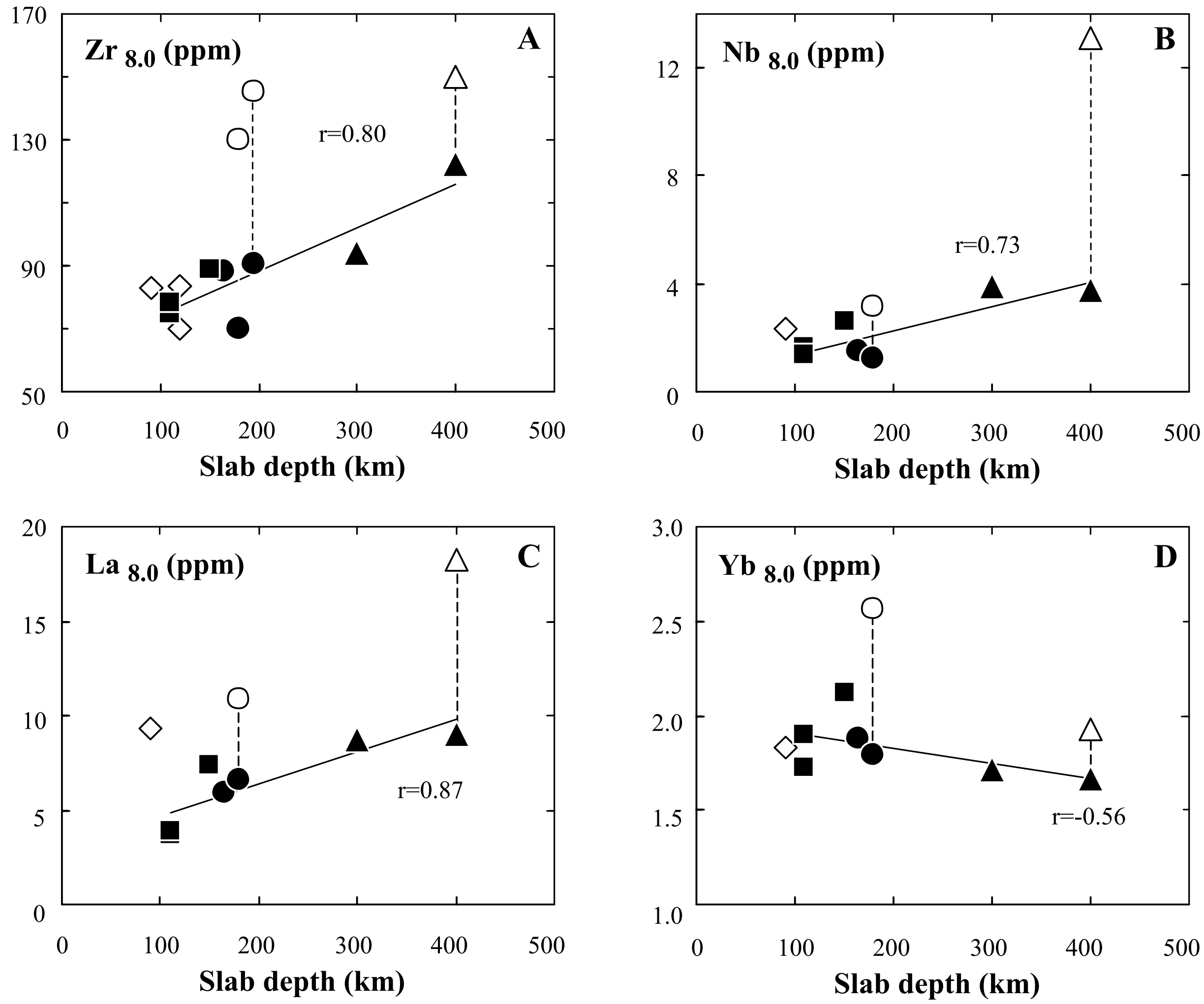

Fig. 2-9
A-D) On 8 % MgO normalized HFSE and REE concentrations of single volcanoes in relation to the depth of the slab surface below the volcano. Positive linear trends exist for $Zr_{8.0}$, $Nb_{8.0}$ and $La_{8.0}$ and a negative trend for $Yb_{8.0}$. However, the trends are less well defined than for the fluid mobile elements (Fig. 2-8). Symbols derived from Fig. 2-2.

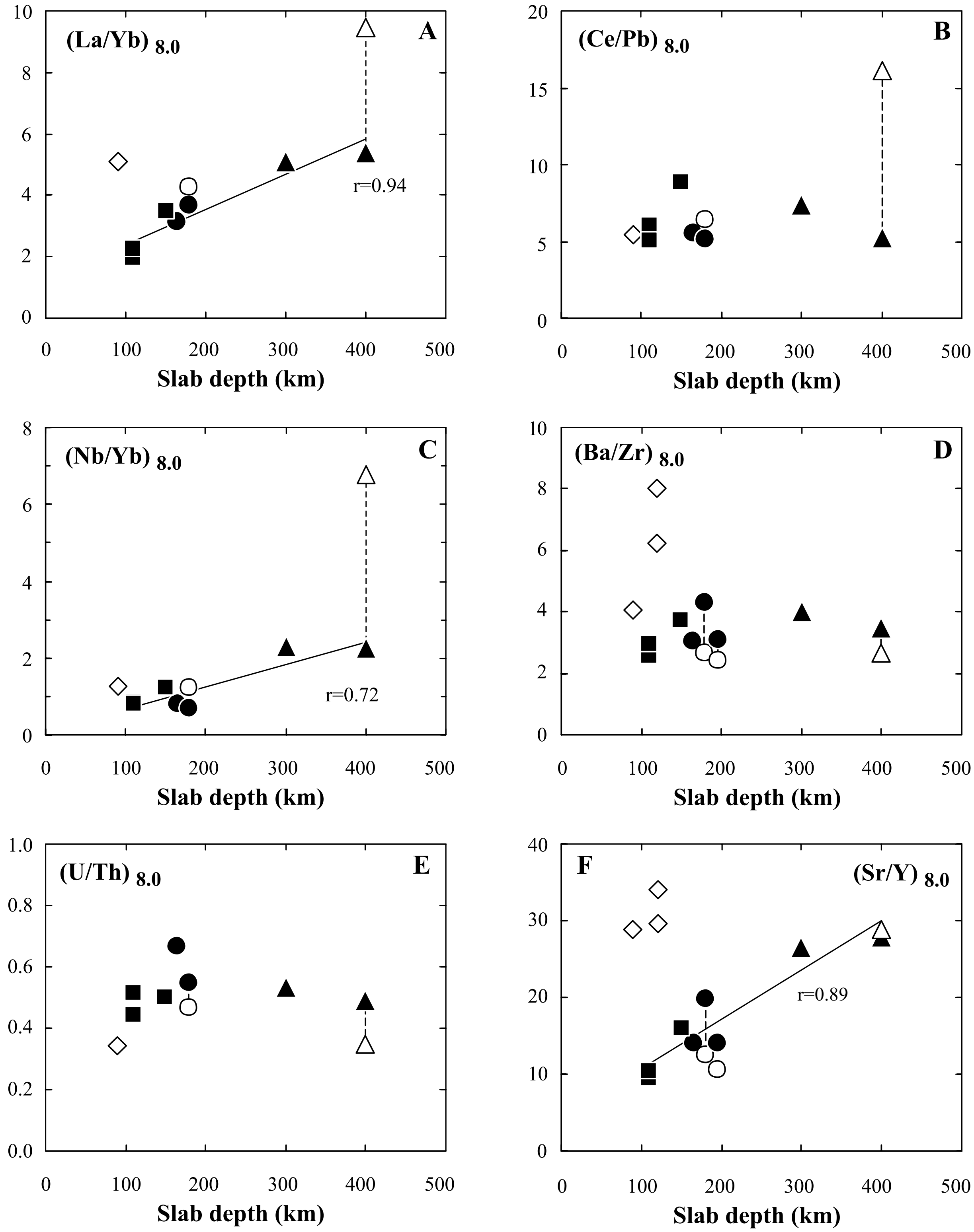

Fig. 2-10

A-F) On 8 % MgO normalized incompatible trace element ratios of single volcanoes in relation to the depth of the slab surface below the volcano. Positive linear trends exist for $(La/Yb)_{8.0}$, $(Nb/Yb)_{8.0}$ and $(Sr/Y)_{8.0}$. The $(Ce/Pb)_{8.0}$, $(Ba/Zr)_{8.0}$ and $(U/Th)_{8.0}$ ratios do not show regular trends. Symbols derived from Fig. 2-2.

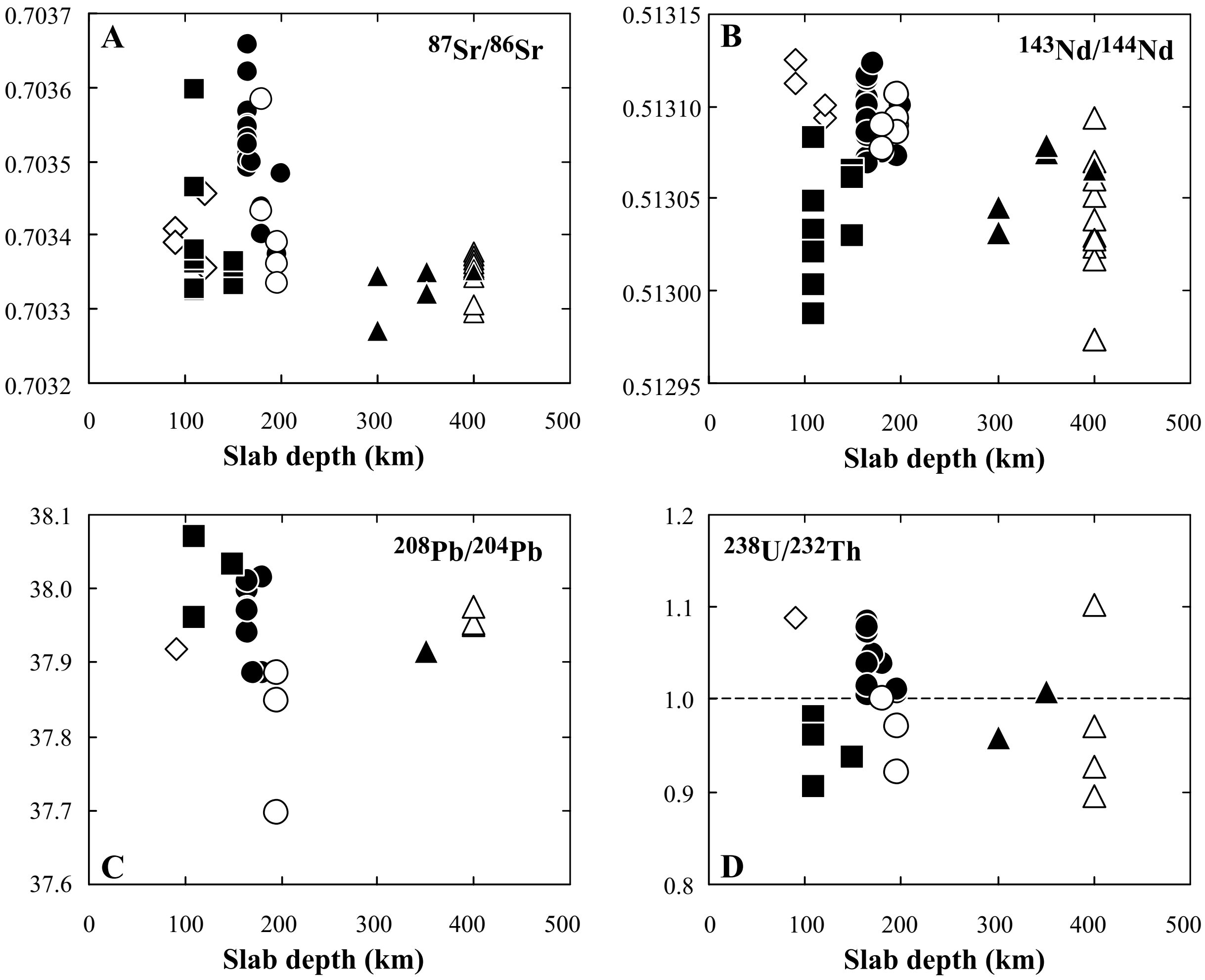

Fig. 2-11

A-D) Variation of isotopic ratios in relation to the depth of the slab surface. Symbols like in Fig. 2-2.

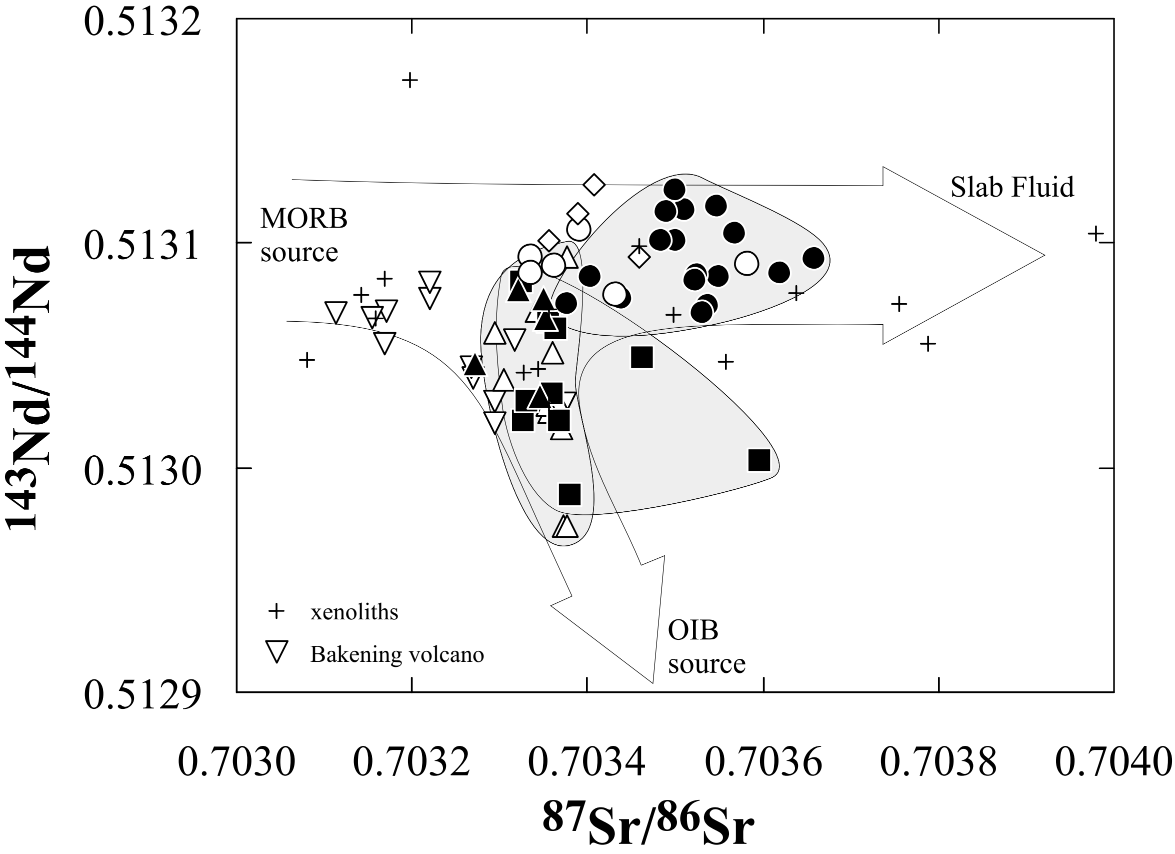

Fig. 2-12

$^{143}Nd/^{144}Nd$ versus $^{87}Sr/^{88}Sr$ for volcanic rocks of Kamchatka. The arrows are drawn schematically to visualize the three-component mixing between MORB, slab fluid and OIB. The data of the Bakening volcano (located ca. 200 km to the south of the transect) and xenolith data (Koloskov et al., 2000) are shown additionally. Other symbols like in Fig. 2-2.

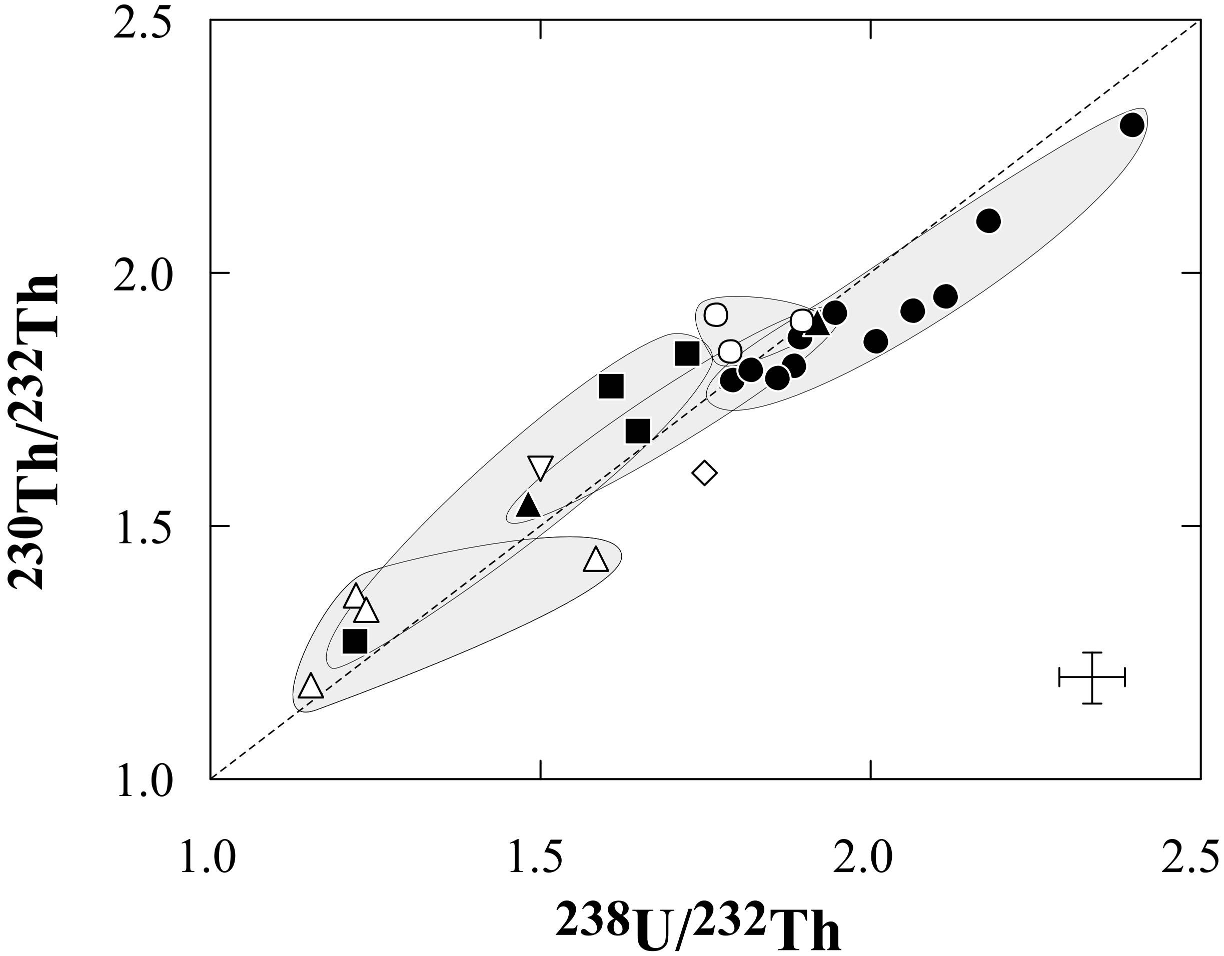

Fig. 2-13
($^{230}Th/^{232}Th$) versus ($^{238}U/^{232}Th$) for Recent and Holocene rocks of the transect. The Kamchatka rocks show a large variation in both ratios, but only a weak positive or negative disequilibrium. The different regions, which form distinct fields with generally either a positive or a negative disequilibrium ratios are separately underlined. The external error is given in the lower right corner. Symbols like in Fig. 2-12.

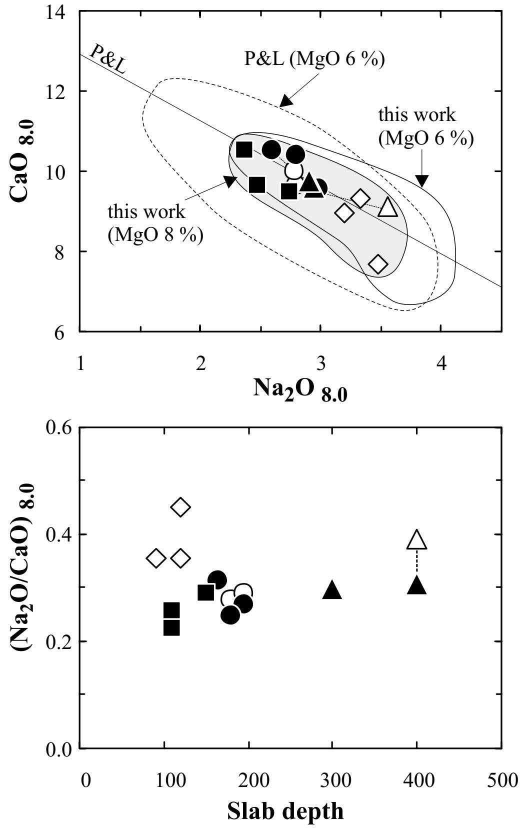

Fig. 2-14
A) $(CaO)_{8.0}$ versus $(Na_2O)_{8.0}$ used in a similar form by Plank and Langmuir (1988) to estimate the melting degree for volcanic front lavas. The field for the on 6 % MgO normalized data of Plank and Langmuir (1988) is compared with our data, normalized on 6 % MgO and 8 % MgO, respectively. There exists a similar but less extended variation for the whole data set from Kamchatka. However, the variation is limited if only the typical arc magmas (black symbols) are regarded. Symbols like in Fig. 2-12.

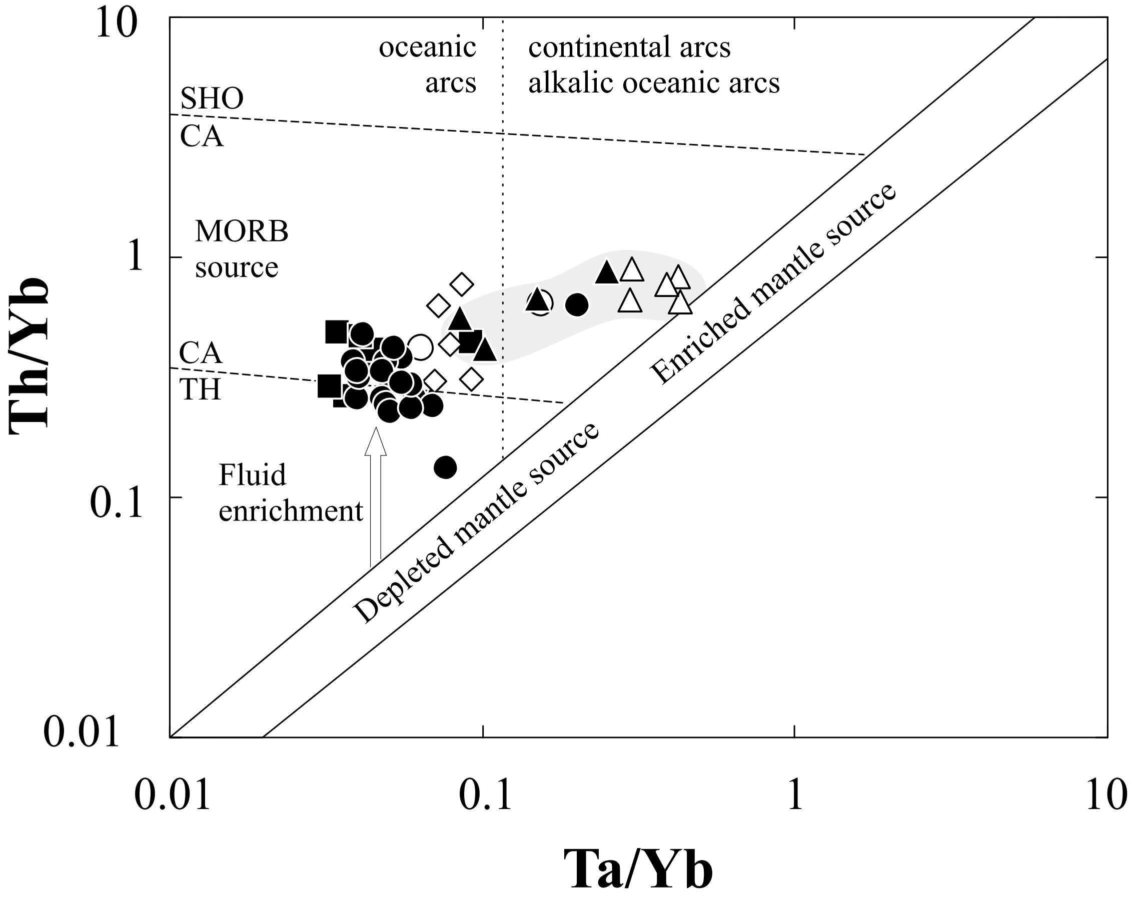

Fig. 2-15
Bivariate plot of Th/Yb vs. Ta/Yb (A) after Pearce (1983). Nearly all samples from the CKD and EVF fall into the field of rocks from oceanic arcs, which were formed from a depleted mantle source. In difference the SR samples tend to an enriched mantle composition, which is underlined by the gray field, enclosing these rocks. The high-K calc-alkaline rocks and the samples from the NCKD have also a slightly Th and Ta enriched composition. Symbols like in Fig. 2-12.

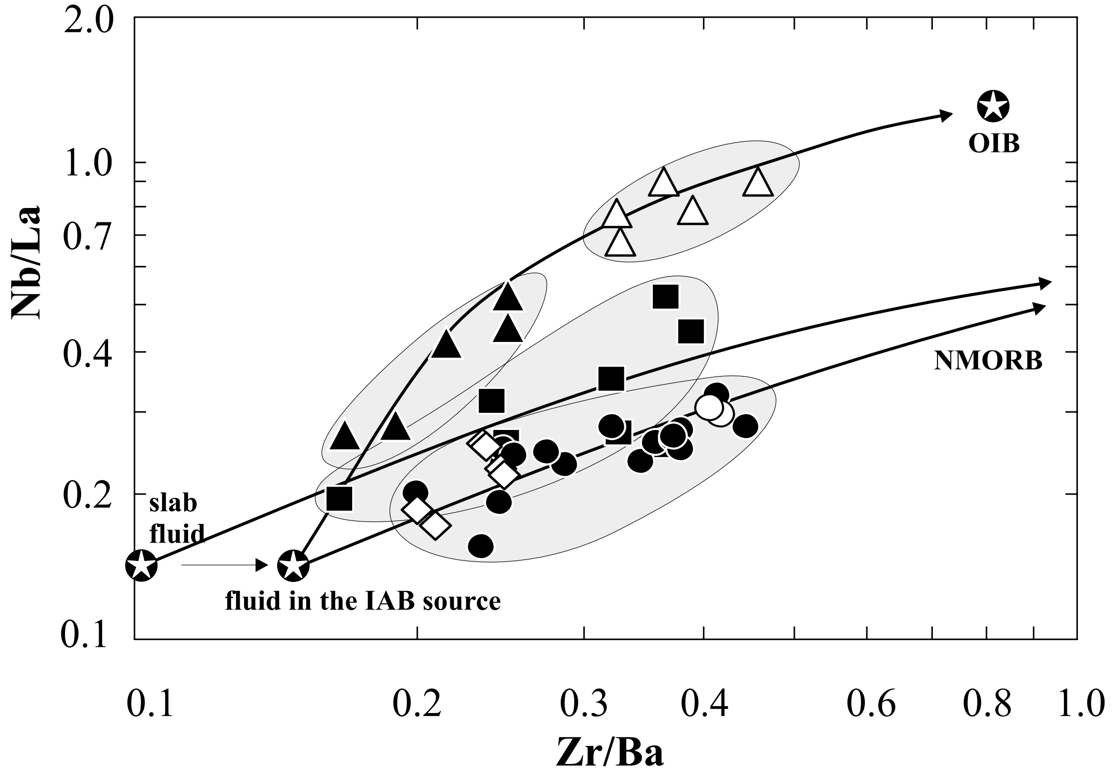

Fig. 2-16
Bivariate plot of Na/La vs. Zr/Ba after Molzahn et al. (1996). The compositions of OIB, NMORB were derived from Sun and McDonough (1989) and for the slab fluid from Brenan et al. (1995; Stalder et al. (1998). This slab fluid will change its composition, when it interacts with the mantle on its way from the slab surface to the melting region, which is suggested by the arrow to the assumed fluid composition in the island arc source. The CKD and SR samples can be explained by interaction with a NMORB and an OIB source, respectively. The EVF lavas lie between these two trends, suggesting a mixture of an OIB and NMORB components with the slab fluid in their source. Alternatively the EVF lavas can be derived from mixing with a more Ba-rich fluid.

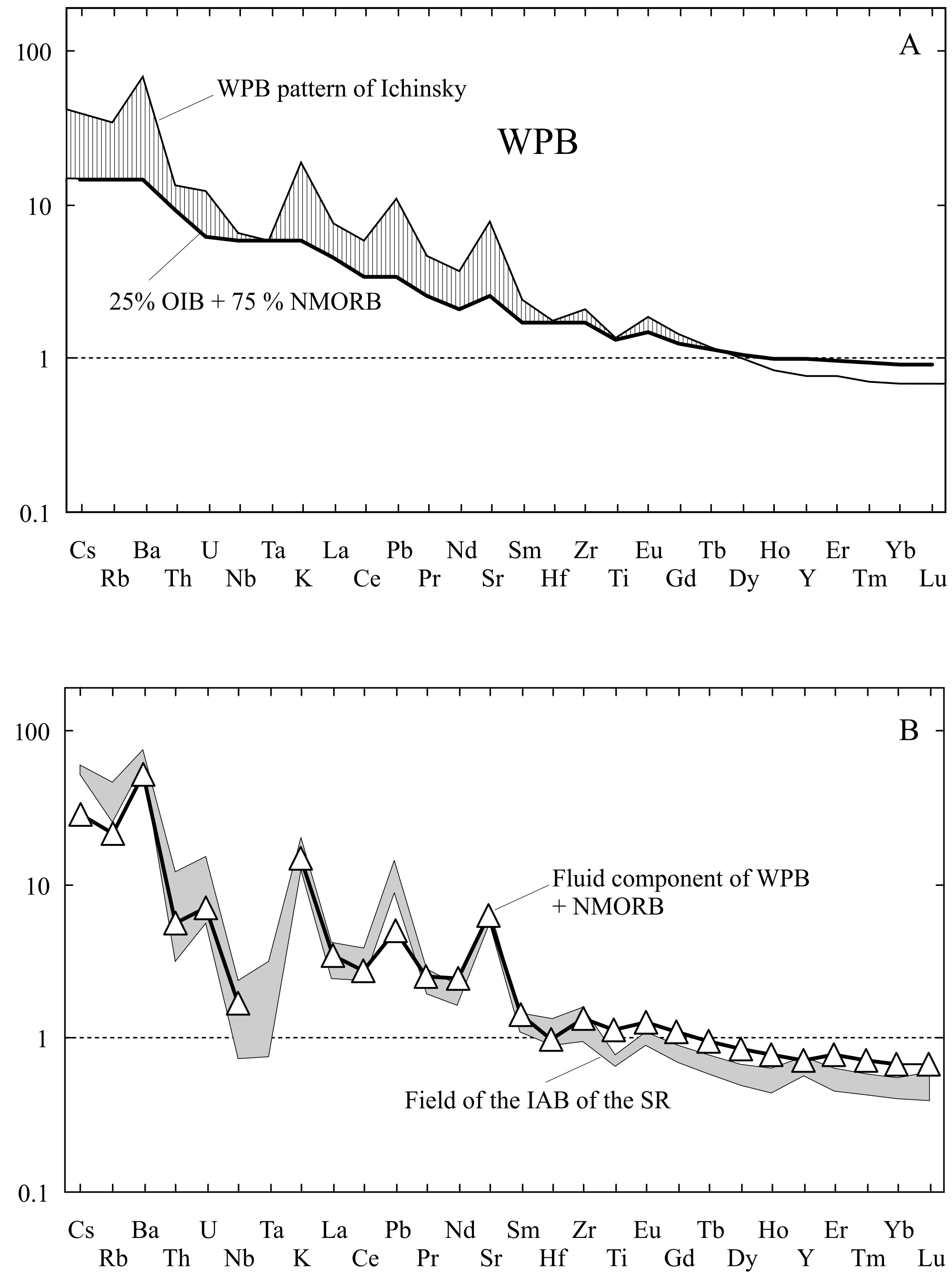

Fig. 2-17
A) Estimation of the fluid component in the WPB of the SR after the approach used by Pearce (1983). In difference to him, we calculated the within-plate component as a mixture of OIB and NMORB (Sun and McDonough, 1989). The hatched field represents the fluid enrichment of this calculated within-plate source, which is necessary to produce the WPB from Ichinsky (average of all analyses > 6 % MgO).
B) The amount of trace elements from the fluid phase was added to the NMORB composition to derive a pattern comparable to the typical arc rocks (composition field). The agreement is surprisingly.